ARTICLE INFO
Article ID: 14-12-01-0006

doi:10.4271/14-12-01-0006

A Data-Driven Greenhouse Gas Emission Rate Analysis for Vehicle Comparisons

Tristan Burton,[1] Scott Powers,[2] Cooper Burns,[1] Graham Conway,[3] Felix Leach,[4] and Kelly Senecal[1]

[1]Convergent Science, Inc, USA
[2]Los Angeles Dodgers, USA
[3]Southwest Research Institute, USA
[4]University of Oxford, UK

Abstract

The technology focus in the automotive sector has moved toward battery electric vehicles (BEVs) over the last few years. This shift has been ascribed to the importance of reducing greenhouse gas (GHG) emissions from transportation to mitigate the effects of climate change. In Europe, countries are proposing future bans on vehicles with internal combustion engines (ICEs), and individual United States (U.S.) states have followed suit. An important component of these complex decisions is the electricity generation GHG emission rates both for current electric grids and future electric grids. In this work we use 2019 U.S. electricity grid data to calculate the geographically and temporally resolved marginal emission rates that capture the real-world carbon emissions associated with present-day utilization of the U.S. grid for electric vehicle (EV) charging or any other electricity need. These rates are shown to be relatively independent of marginal demand at the highest marginal demand levels, indicating that they will be relatively insensitive to the addition of renewable electricity generation capacity up to the point at which curtailment occurs regularly unless the most carbon-intensive electricity sources are preferentially deactivated. We propose a simplified methodology for comparing emissions from BEVs and hybrid electric vehicles (HEVs) based on the marginal emission rates and other publicly available data and apply it to comparative case studies of BEVs and HEVs. We find that currently there is no evidence to support the idea that BEVs lead to a uniform reduction in vehicle emission rates in comparison to HEVs and in many scenarios have higher GHG emissions. This suggests that a mix of powertrain technologies is the best path toward reducing transportation sector emissions until the U.S. grid can provide electricity for the all-electric fleet infrastructure and vehicle operations with a carbon intensity that produces a net environmental benefit.

History

Received: 14 Sep 2021
Revised: 14 Feb 2022
Accepted: 29 Mar 2022
e-Available: 13 Apr 2022

Keywords

Battery electric vehicle, Hybrid electric vehicle, Life-cycle analysis, Electricity grid, Greenhouse gases, Marginal emission rate

Citation

Burton, T., Powers, S., Burns, C., Conway, G. et al., "A Data-Driven Greenhouse Gas Emission Rate Analysis for Vehicle Comparisons," *SAE Int. J. Elect. Veh.* 12(1):2023, doi:10.4271/14-12-01-0006.

ISSN: 2691-3747
e-ISSN: 2691-3755

Introduction

The global vehicle market is undergoing substantial changes in technology, motivated by a recognition of the importance of reducing greenhouse gas (GHG) emissions from the vehicle fleet. As part of this transition, alternatives to the internal combustion engine (ICE) such as battery electric vehicles (BEVs) are being developed. In addition, technologies such as high-efficiency internal combustion engine vehicles (ICEVs), full hybrid electric vehicles (FHEVs), and plug-in hybrid electric vehicles (PHEVs) [1], are being advanced [2, 3].

Globally, regulators today require that vehicular emissions are measured at the tailpipe. This method ensures that most of the vehicular emissions generated while driving are appropriately quantified[1]. There are two main limitations associated with tailpipe-only emissions measurements. Firstly, tailpipe-only measurements omit emissions generated during vehicle production and end-of-life processes. Secondly, fuel-cell electric vehicles emit only water from their tailpipe, and BEVs have no tailpipe, therefore no emissions are measured. However, this does not consider the emissions produced when creating their primary energy sources: hydrogen and electricity, respectively.

An emissions-based life-cycle analysis (LCA) quantifies total emissions generated throughout the entire vehicle life. These include, but are not limited to, emissions associated with vehicle and powertrain production, vehicle use, end-of-life destruction, and recycling, as well as emissions generated during the manufacture and transport of hydrocarbon-based fuels, hydrogen, and electricity [4]. Battery production is an energy-intensive process [5] and excluding this contribution for the BEV will produce biased results. A similar error occurs by neglecting the emissions associated with petroleum extraction, refining, and fuel delivery [6] for an ICEV. Many of the contributions from both production and operation are associated with electricity utilization. Therefore, the electricity emission rate is possibly the term that requires the highest accuracy in the calculation of total GHG emissions [7].

In most cases of interest, the required electricity is delivered by a coupled network of regional grids utilizing a variety of energy sources, both emitting and non-emitting. The electricity mix is often analyzed in a similar fashion to the familiar probability problem of sampling with replacement from a jar. This interpretation of electricity supply leads to the average or total mix emission rate [7], i.e., electrons from the various sources of electricity are drawn with probabilities equal to the fractional total supply of those sources over some relevant time period of interest. However, a more representative description of the electricity supply process would include many draws from a group of electrical loads occurring simultaneously with replacements from another group of electrical loads and a jar with constantly changing probabilities for the electricity sources depending on the balance between the two groups (i.e., total demand) and other factors such as time of day. The average mix emission rate is not expected to be accurate for this more realistic scenario, and the emissions and grid data confirm that this is indeed the case for the U.S. grid.

Recent publications suggest that the only available option to substantively reduce emissions in the transportation sector is to rapidly adopt BEVs [8, 9]. With substantial grid decarbonization, BEVs will most likely eventually supersede other powertrain technologies in terms of reducing GHG emissions. However, the state of readiness of the U.S. grid for all-electric fleets remains an open question that can only be answered with careful analysis of available grid data. While many studies supporting the rapid transition to all-electric light-duty vehicle fleets focus on comparisons between BEVs and ICEVs, the most relevant alternatives to the BEV for emissions reduction are FHEVs and PHEVs. The primary goal of this study is to investigate the conditions under which the BEV or one of these alternatives provides the greatest emissions reduction benefit.

The argument for all-electric vehicle fleets is that the GHGs produced in the production, operation, and end-of-life phases by these vehicles are less than the corresponding GHG emissions from other powertrain technologies. This argument is more compelling when the GHG contributions from the electricity production sector are calculated with average mix emission rates that are inconsistent with the U.S. electricity supply process and associated grid data. In this work, we apply physically representative modeling to reveal the source of the error associated with the average mix emission rate and develop a methodology for calculating the more representative marginal emission rates using available grid data. Details of the methodology are discussed within the context of the California grid before presenting geographically and temporally resolved marginal emission rates for the entire contiguous U.S. grid. Finally, the marginal emission rates are applied using a practical vehicle comparison methodology to identify the conditions under which the various powertrain technologies are superior from a GHG environmental impact perspective.

Electricity Emission Rates

The U.S. Energy Information Administration (EIA) provides a source breakdown of the 2019 U.S. total of 4117 TWh of electricity generation [10]. The major energy sources for the U.S. grid in 2019 were natural gas (38.4%) coal (23.5%), nuclear (19.7%), hydropower (hydro) (10.7%), renewables (7.0%), and petroleum (1%). Natural gas, coal, and petroleum accounted for 63% of the electricity generation while they were responsible for nearly 99% of the carbon dioxide produced by the total electricity generation [11]. The carbon intensities for natural gas, coal, and petroleum are 0.42 kilogram carbon dioxide equivalent per kilowatt-hour (kg CO_2eq/kWh), 1.00 kg

[1] One additional source of emissions not measured is in the form of particulate matter from brakes, tires, and road wear.

CO_2eq/kWh, and 0.96 kg CO_2eq/kWh, respectively [12]. This yields a weighted average for the average mix of 0.41 kg CO_2eq/kWh. This value, or one close to it, is typically used for U.S.-based LCA calculations when considering the GHG contribution of electric vehicles (EVs) [13, 14].

Another electricity mix to consider is the marginal mix. In the marginal mix, the sources of electricity that are brought online as demand increases (or taken offline as demand decreases) are considered to determine the appropriate emissions intensity for loads on the grid. The grid power demand is usually met using the lowest cost mix possible [15]. In many cases the lowest cost mix is the lowest carbon intensity mix as non-emitting sources have low fuel costs, although coal has fallen out of favor in many U.S. regions recently due to the associated emissions. As more power is needed, this merit order dictates that capacity is taken from the next cheapest source, as illustrated in Figure 1, for a grid where coal and gas are the primary marginal sources at a particular time and oil is only utilized at the highest demand levels. Other factors impacting the marginal mix are availability, startup costs, ramping rate constraints, and minimum up-time [16].

Several studies have utilized both the average and marginal electricity mix emission rates in their calculations [7]. Studies that do utilize a marginal mix often show BEVs to have significantly higher emissions than when using the average mix. One study using a projected UK marginal mix in 2015 found that the life-cycle carbon dioxide (CO_2) emissions of a BEV can be 23% higher than an ICEV and 30% higher than an FHEV whereas, using the average mix, the BEV produces 20% less emissions [17]. A U.S.-focused study compared three hypothetical electricity scenarios of marginal, average, and 100% solar on a state-by-state basis [18]. It found that when using the average electricity mix, the life-cycle CO_2 of a BEV was favorable in 24 states. When switching to a marginal mix, however, the BEV was favorable in zero states while the PHEV had the lowest GHG emissions in 17 states and the FHEV in the remaining 33 states. Another U.S.-based study focused on 30 km, 60 km, and 90 km range PHEVs as a replacement to conventional ICEVs and a competitor to FHEVs. It found that using the average mix

FIGURE 1 Illustration of marginal cost versus demand.

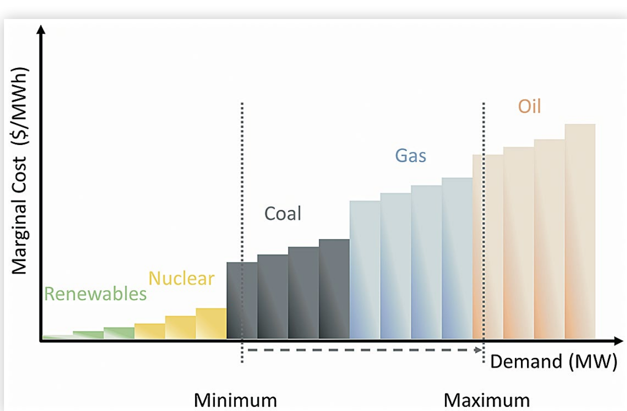

PHEVs were superior to FHEVs; however, when moving to a higher carbon-intensity marginal grid, all PHEV variants had higher life-cycle emissions than FHEV equivalents [19]. It should be noted that this paper used a 2008 U.S. average grid intensity of 0.67 kg CO_2/kWh, which is significantly higher than the 2020 value. This does not impact the marginal case result but rather implies the PHEVs would be much better than FHEVs by 2020 standards if the average mix was used. This highlights the challenges of using the current mix (average or marginal) when predicting 10-20-year LCA studies.

Consider the set of demand Scenarios A and B with instantaneous electricity demand levels, D_A and D_B (in MW), separated by a constant magnitude due to the addition or removal of a known load, ΔD_{AB}. The expected value of the change in the total grid GHG emission mass flow rate (in kg CO_2eq/h) between the scenarios can be written in terms of the sum of the GHG emissions from N electricity sources at the two demand levels as follows:

$$E\left[\Delta GHG_{AB}\right] = E\left[GHG_B - GHG_A\right] = E\left[\sum_{i=1}^{N} GHG_{B_i}\right] - E\left[\sum_{i=1}^{N} GHG_{A_i}\right] \quad \text{Eq. (1)}$$

where the expectation is with respect to the uncertainty between the emission mass flow rate for each source and D_A, and the expected value of the grid emission rate is obtained by dividing through by ΔD_{AB}:

$$ER_{AB} = \frac{E\left[GHG_B - GHG_A\right]}{D_B - D_A} \quad \text{Eq. (2)}$$

The average mix emission rate is obtained from Equation 2 using the assumption that all electricity sources are demand-responsive so that, at every D_A, the ratios of the individual electricity sources are fixed. However, power plants are activated and deactivated based on the merit order (see Figure 1), and many electricity sources do not respond to demand. As such, there is no constraint on the fractions of the electricity generation sources. To obtain a more representative emission rate that accurately accounts for the appropriate demand-responsiveness of the individual electricity sources, regression of power plant emissions data over the full range of electricity demand in a particular region at a particular time is applied. We will refer to this emission rate as the marginal emission rate.

To further elucidate the difference between emission rates, Figure 2 shows illustrative examples of emission mass flow rate versus electricity demand curves at the same hour of the day on three different days. The total demand is met by four sources, each with a different average carbon intensity represented by its slope. On different days and demand levels, the portion of the demand covered by each source will change. The line segments are ordered by their carbon intensity, but that does not imply that Source 4 will be the only one to accommodate demand changes. For the three total demand

FIGURE 2 Sample present-day emission mass flow rate curves.

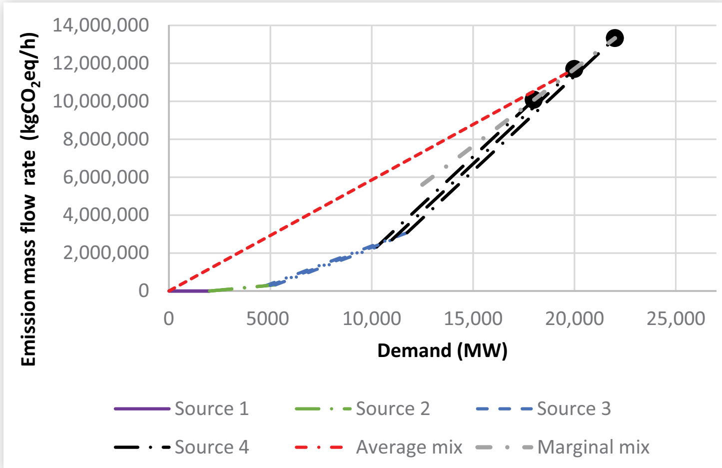

levels in Figure 2, only Source 3 and Source 4 (e.g., coal and natural gas) adjust consistently with demand, while Source 2 (e.g., solar) makes small random changes, and Source 1 (e.g. nuclear) does not change. The slope of the marginal electricity mix line produced by fitting the three endpoints is the marginal emission rate, and the data used to produce it includes much of the complexity of the grid operation for the local region at this hour of the day.

The average electricity mix line in Figure 2 demonstrates consistent underprediction of the magnitude of the change in the emission mass flow rate for loads added or removed from the grid. At a more fundamental level, the average mix emission rate does not consider the fact that removing something from the grid has an outsized benefit in terms of reducing emissions because, in most cases, some of the more carbon-intensive sources will drop faster with demand while the non-emitting sources do not change at all. There is no reason to turn off solar or wind when demand drops (unless it might overload the grid) because the fuel is free and full utilization of renewable capacity guarantees minimization of total GHG emissions.

Figure 2 shows that the average mix emission rate is representative of the grid emissions data at only two demand values, the average-demand value and the zero-demand value. Therefore, the environmental opportunity cost calculation that was initially intended for a load of interest is effectively converted to an environmental opportunity cost calculation for the entire grid demand. This means that the average mix emission rate prediction of the emissions is wrong for every load individually, but when applied to the entire grid demand at once, it can produce the correct global result. The use of an average mix emission rate reduces the potential emissions penalty associated with increased demand on the grid and diminishes the corresponding benefit associated with the reduction of grid demand. The linear regressions used here to calculate the marginal emission rate capture the emission mass flow rate demand sensitivity better over the demand range of interest, but care must be taken when considering large load changes as the marginal mix may be different at substantially different demand levels depending on the grid management. It is for this reason that the marginal mix line in Figure 2 is only plotted over the relevant demand range for the grid.

As vehicles purchased today may have 15- to 20-year lifetimes and the carbon intensity of the grid will likely drop during that time, the results of a vehicle LCA will be affected by grid emission rate changes. However, utilization of the average mix emission rate for projections of future grid emissions incurs the same errors as the present-day grid and compounds them with the associated uncertainty of predicting future grid operation. We consider a future grid that is meeting higher demand levels due to the growth of an EV fleet and that has replaced a large fraction of the highest carbon intensity electricity in Figure 3. Comparing to Figure 2 shows that total emissions have dropped, but the emission rate discrepancy between average mix and marginal persists, although both slopes have decreased. If the renewables were increased further, minimal utilization of Source 4 would be required, and the marginal emission rate would fall substantially. As future power plant data is not available, incorporating these effects accurately requires modeling of future grids including projected demand response and renewable generation capacity rather than assumptions of electricity fractions for the different sources. Such studies have been performed [20] and reveal that the grid requirements for charging a future EV fleet are more complicated than solely adding renewables [21].

Marginal Emission Rate Calculation Methodology

The datasets used in this work to determine the marginal emission rate consist of observations from power plants distributed across the contiguous U.S. and aggregated regional

FIGURE 3 Sample future emission mass flow rate curves with increased demand and high renewable electricity generation.

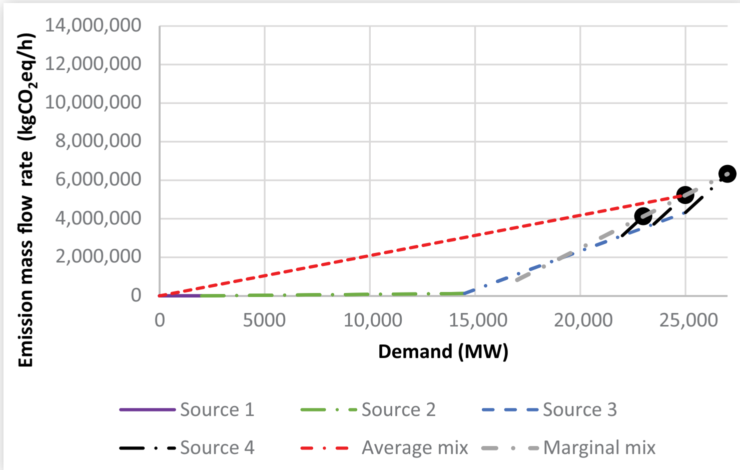

data. We use P to denote the set of power plants present in the data, R to denote the set of geographic regions, and U to denote the set of sources (gas, hydro, solar, etc.) used by the power plants to generate electricity. Each power plant $p \in P$ belongs to a geographic region $r \in R$ and uses one source $u \in U$ to generate electricity. We use P_{ru} to denote the set of power plants which generate electricity using source u in region r. The observations typically reflect averages over one-hour windows, and we denote the set of observation hours as H. For example, the observation hour $h = 9$ reflects the one-hour period between 8 a.m. and 9 a.m. The observations are repeated each day for N = 365 days, throughout the calendar year.

For some power plants (belonging to the set denoted by $Q_{ru} \subseteq P_{ru}$), we observe hourly data on the electricity supply and emissions generated, that is, for each $p \in Q_{ru}$, $h \in H$, $i \in \{1, \ldots, N\}$, we observe S_{phi} (the electricity supply in MW) and E_{phi} (the emission mass flow rate, in kg CO_2/hour). For the rest of the power plants (this set is denoted by $Q'_{ru} \subset P_{ru}$), we do not observe hourly supply and emissions. However, we observe the aggregated hourly electricity supply by source across the region, and this allows us to calculate the total electricity supply by hour across all plants belonging to Q'_{ru}. We denote this by S'_{ruhi}, and we denote the total supply in region r from source u during hour h of day i as

$$S^*_{ruhi} = S'_{ruhi} + \sum_{p \in Q_{ru}} S_{phi} \qquad \text{Eq. (3)}$$

In addition to the data we observe within each region, we also observe data on electricity supply transferred between regions. Regions may import electricity supply from a neighboring region to meet high demand or may have agreements in place that result in the regular transfer of electricity supply between them. For each adjacent region to r, $q \in R_r$ we observe T_{rqhi}, the electricity supply transferred to region r from region q during hour h of day i.

We define the total demand in each region to be equal to the combination of local demand within the region and any demand from other regions that is satisfied by a transfer of electricity, i.e., exports. The total demand in each region is balanced by the supply generated locally along with electricity imported by the region. Using D_{rhi} to denote the local demand on region r during hour h of day i, the total demand for each region, D^*_{rhi}, is defined as

$$D^*_{rhi} \equiv D_{rhi} + \sum_{q \in R_r} T_{qrhi} = \sum_{u \in U} S^*_{ruhi} + \sum_{q \in R_r} T_{rqhi} \qquad \text{Eq. (4)}$$

and is balanced by the total supply and imports.

Step 1: Estimate Total Emissions by Hour

As we have hourly emissions data for each plant in Q_{ru} but not for the plants in Q'_{ru}, and for most regions and sources, the plants in Q_{ru} typically represent 75-100% of the total source generation, we use the data from plants in Q_{ru} to determine a representative emission rate by hour and then apply these estimates to the total supply data for the plants in Q'_{ru} to estimate the total emission mass flow rate from Q'_{ru}. Specifically, our model for each hour h and day i is

$$\sum_{p \in Q_{ru}} E_{phi} = \gamma^E_{ruh} \sum_{p \in Q_{ru}} S_{phi} + \epsilon^E_{ruhi} \qquad \text{Eq. (5)}$$

where γ^E_{ruh} is an unknown parameter, and the ϵ^E_{ruhi} are independent, normally distributed error terms with zero mean and unknown variance. We first estimate γ^E_{ruh} by fitting a linear regression model, resulting in $\hat{\gamma}^E_{ruh}$. Then we estimate the emission mass flow rate for all Q'_{ru} as $\hat{\gamma}^E_{ruh} S'_{ruhi}$. We fit this model separately for each region r and source u (allowing for the variance of ϵ^E_{ruhi} to depend on the region and source).

The resulting estimated total emission mass flow rate (Y^G_{rhi}) for the generation in region r during hour h on day i is

$$Y^G_{rhi} \equiv \sum_{u \in U} \left(\hat{\gamma}^E_{ruh} S'_{ruhi} + \sum_{p \in Q_{ru}} E_{phi} \right) \quad \text{Eq. (6)}$$

Step 2: Classify Marginal Sources and Imports

To calculate the emission rate for a load added to a grid, it is important to distinguish those sources that can provide for the additional electricity request in each region, i.e., the marginal sources. A source is marginal if an increase in electricity demand in a region corresponds with an increase in electricity generation from the source. A source is non-marginal if an increase in demand does not correspond to an increase in generation from the source. The same goes for imports: the electricity supply imported to region r from region q is marginal if and only if an increase in demand in region r corresponds with an increase in the quantity of this import from region q.

There are a number of previously published methodologies [22, 23, 24, 25] for making the selections of the sources that are marginal. In the present work, we base the classification primarily on evidence from the data. Within each region r, source u, and hour h, we perform a linear regression of the supply generated from the source on the total demand in the region. Specifically, our model is that, for all days i,

$$S^*_{ruhi} = \alpha^S_{ruh} + \beta^S_{ruh} D^*_{rhi} + \epsilon^S_{ruhi} \quad \text{Eq. (7)}$$

where α^S_{ruh} and β^S_{ruh} are unknown parameters, and the ϵ^S_{ruhi} are independent, normally distributed error terms with zero mean and unknown variance. The key parameter in this regression is β^S_{ruh}; if it is negative or zero, the interpretation is that, in region r, the source u is non-marginal during hour h because its supply does not increase with total demand. If β^S_{ruh} is positive, this means that, in region r, source u is marginal during hour h because its supply increases as total demand increases.

We perform a similar linear regression to classify imports as marginal or non-marginal. Within each import region r, adjacent region q, and hour h, our model is that, for all days i,

$$T_{rqhi} = \alpha^T_{rqh} + \beta^T_{rqh} D^*_{rhi} + \epsilon^T_{rqhi} \quad \text{Eq. (8)}$$

where α^T_{rqh} and β^T_{rqh} are unknown parameters, and the ϵ^T_{rqhi} are independent, normally distributed error terms with zero mean and unknown variance. The interpretation is the same as the previous model. If β^T_{rqh} is negative or zero, then imports to region r from region q are non-marginal during hour h.

After estimating the regression models described in Equations 7 and 8, we follow two different definitions of marginal/non-marginal classification and report the results for both methods. According to the *Statistically Significant Source* marginal classification, a source is marginal for a particular region and hour if the corresponding estimate for β^S_{ruh} is greater than 0.01, and the p-value is less than 5% for the hypothesis that $\beta^S_{ruh} = 0$. The classification for imports follows the same rule based on β^T_{ruh}. Note that, according to this definition, the same source or import may be marginal at one time of day and non-marginal at another time of day. Our alternative rule, the *Emitting Source* marginal classification, is identical to the *Statistically Significant Source* classification, except that we do not allow non-emitting sources to be classified as marginal. Regardless of which classification we use for marginal/non-marginal sources, the result is that, for each region r and hour h, we have a partition of U into U^M_{rh} (marginal sources) and U^N_{rh} (non-marginal sources). Similarly, we have a partition of the r-adjacent regions into R^M_{rh} (marginal import regions) and R^N_{rh} (non-marginal import regions).

In nearly all cases, the emitting sources are marginal. In situations where an emitting source is non-marginal, we remove its contribution to the total generation emission mass flow rate in Equation 6. On the other hand, nuclear is considered non-marginal in all cases as it cannot respond to any demand changes. The *Statistically Significant Source* marginal classification permits sources such as hydro, solar, and wind to meet a portion of a demand increase even though they are capacity limited or are intermittent. Therefore, we consider this classification to produce a lower bound for the emission rate. In general, coefficients of determination (R^2) from the regressions against total demand are relatively high (>0.7) for emitting sources and hydro, moderate (0.4-0.7) for many imports, and relatively low (<0.4) for solar and wind. As a result, when solar or wind is marginal, we anticipate lower demand-response-based emission rates, but greater uncertainty in the results from the regressions. For the *Emitting Source* marginal classification, only the statistically significant imports are assigned to the marginal category along with the marginal emitting sources. Therefore, the emitting source marginal classification will produce an upper bound for the emission rate.

Step 3: Estimate Relationship between Emission Mass Flow Rate and Demand

Our motivation for identifying non-marginal sources in Step 2 is that, by removing these sources, we get more precise (less noisy) estimates for the relationship between demand and marginal electricity supply. Specifically, rather than focusing on demand, we focus on the demand that has not been met by the non-marginal supply, i.e., the marginal demand:

$$X_{rhi} \equiv D^*_{rhi} - \sum_{u \in U^N_{rh}} S^*_{ruhi} - \sum_{q \in R^N_{rh}} T_{rqhi} \quad \text{Eq. (9)}$$

Now we consider the question: If the current marginal demand on region r during hour h is some value x, what will be the result from introducing an additional incremental demand of Δx? We are interested in knowing the expected emission mass flow rate given a marginal demand of $x + \Delta x$, in contrast with a marginal demand of x. Note that if we are introducing this marginal demand to region r, we are not interested only in the resulting emissions in region r but also in the resulting emissions in other regions (in case the increase in demand leads to an increase in imports). We wish to know for each hour h the change in the combined emission mass flow rate, $Y_{rh} \equiv Y_{rh}^{G} + \sum_{q \in R_{rh}^{M}} Y_{qh}^{T}$,

$$E\left[Y_{rh}^{G} + \sum_{q \in R_{rh}^{M}} Y_{qh}^{T} | X_{rh} = x + \Delta x\right] - E\left[Y_{rh}^{G} + \sum_{q \in R_{rh}^{M}} Y_{qh}^{T} | X_{rh} = x\right] \qquad \text{Eq. (10)}$$

where Y_{qh}^{T} is the emission mass flow rate in the adjacent region q providing marginal imports to r. Here the expectation is with respect to the daily uncertainty between marginal demand and emission mass flow rate. First, we estimate the relationship between the marginal demand and the emission mass flow rate from generation in the same region, that is, we focus on

$$E\left[Y_{rh}^{G} | X_{rh} = x + \Delta x\right] - E\left[Y_{rh}^{G} | X_{rh} = x\right] \qquad \text{Eq. (11)}$$

We make the key assumption that, within the range of x and $x + \Delta x$, the relationship between Y_{rh} and X_{rh} is linear. This corresponds to the assumption that, for a fixed hour h, the emission mass flow rate lies on a line segment, although the slope of the line is not tied to any individual source as shown by the end points of the emission mass flow rate curves in Figure 2. Our linear regression model for each region r and hour h is that, for all days i,

$$Y_{rhi}^{G} = \alpha_{rh}^{Y} + \beta_{rh}^{Y} X_{rhi} + \epsilon_{rhi}^{Y} \qquad \text{Eq. (12)}$$

where α_{rh}^{Y} and β_{rh}^{Y} are unknown parameters, and the ϵ_{rhi}^{Y} are independent, normally distributed error terms with zero mean and unknown variance. From this model it is easy to calculate the expression from Equation 11:

$$\begin{aligned} &E\left[Y_{rh}^{G} | X_{rh} = x + \Delta x\right] - E\left[Y_{rh}^{G} | X_{rh} = x\right] \\ &\quad = \left(\alpha_{rh}^{Y} + \beta_{rh}^{Y}\left(x + \Delta x\right)\right) - \left(\alpha_{rh}^{Y} + \beta_{rh}^{Y} x\right) = \beta_{rh}^{Y} \Delta x \end{aligned} \qquad \text{Eq. (13)}$$

In other words, an increase in demand of Δx corresponds to an increase in emission mass flow rate of $\beta_{rh}^{Y} \Delta x$ due to local generation. For each region r and hour h, we estimate $\hat{\beta}_{rh}^{Y}$ by fitting the regression model specified by Equation 12.

Once we have estimated the relationship between marginal demand and local generation emissions within each region, we still need to estimate the relationship between marginal demand in the region of interest and emissions from other regions. For this purpose, we estimate a similar model to Equation 8 with total demand replaced by marginal demand. According to this model, an increase in marginal demand of Δx in region r corresponds to an increase of $\beta_{rqh}^{T} \Delta x$ in imports to region r from region q. In other words, an increase in marginal demand of Δx on region r means that region q needs to provide $\beta_{rqh}^{T} \Delta x$ more electricity supply:

$$\begin{aligned} &E\left[Y_{qh}^{T} | X_{rh} = x + \Delta x\right] - E\left[Y_{qh}^{T} | X_{rh} = x\right] \\ &\quad = E\left[Y_{qh} | X_{qh} = x + \hat{\beta}_{rqh}^{T} \Delta x\right] - E\left[Y_{qh} | X_{rh} = x\right] \end{aligned} \qquad \text{Eq. (14)}$$

Bringing everything together, we have estimated that an increase of Δx in demand in region r corresponds to an increase of $\hat{\beta}_{rh}^{Y} \Delta x$ in the emission mass flow rate from a local generation for region r and an increase in marginal demand of $\hat{\beta}_{rqh}^{T} \Delta x$ for all adjacent regions providing marginal imports $q \in R_{rh}^{M}$. Normalizing the combined result by the additional load produces a coupled system of equations for the marginal emission rates in all regions

$$\begin{aligned} &\frac{E\left[Y_{rh} | X_{rh} = x + \Delta x\right] - E\left[Y_{rh} | X_{rh} = x\right]}{\Delta x} \\ &= \hat{\beta}_{rh}^{Y} + \sum_{q \in R_{rh}^{M}} \hat{\beta}_{rqh}^{T} \frac{E\left[Y_{qh} | X_{qh} = x + \Delta x\right] - E\left[Y_{qh} | X_{qh} = x\right]}{\Delta x} \end{aligned} \qquad \text{Eq. (15)}$$

where linearity of the emission mass flow rate on each exporting grid has been used to convert from a $\hat{\beta}_{rqh}^{T} \Delta x$ basis to the Δx basis. The local generation marginal emission rate can be calculated by dividing $\hat{\beta}_{rh}^{Y}$ by $1 - \sum_{q \in R_{rh}^{M}} \hat{\beta}_{rqh}^{T}$ to remove the dilution caused by the inclusion of the marginal imports in the marginal demand variable. Before using the $\hat{\beta}_{rqh}^{T}$ values in Equation 15 or to calculate the local generation marginal emission rate, we normalize them by a constant so that the combined sum of all the $\hat{\beta}_{rqh}^{T}$ and the $\hat{\beta}_{ruh}^{S}$ for region r in hour h is one. In most cases the unnormalized sum is between 0.99 and 1.01 due to the balance between the supply and demand data used for the regressions.

Two types of least squares linear regression procedures are applied in this work to calculate the parameter estimates for the sources in Equation 7, imports in Equation 8, and the emission mass flow rate in Equation 12, referred to in shorthand here as α and β. The first calculates an α and β value at each h within a month of interest and will be denoted as monthly. The second assumes a single α value at each h within a year of interest while the β values are different for each month at each value of h, and will be denoted as annual. In the first procedure, a linear regression is performed at every h for each source using only the data from an individual month, i.e., 24 regressions per month for each source, import, and the emission mass flow rate, where each regression produces a single α and β value. In the second procedure, a linear regression is performed at every h for each source using the data from an entire year, i.e., 24 regressions for each source where each regression produces a single β value and 12 α values, one for each month. The first procedure allows for marginal emission rates that vary month to month but uses a relatively small sample size, e.g., 30 samples, while the second procedure leads to loss of granularity but utilizes a larger sample size, e.g., 300 samples. In both cases, we exclude data points from the regressions that do not satisfy a balance between demand and the sum of the individual sources within a specified tolerance. Here we only present results from annual regressions. The monthly regression results were used to validate the annual regression results by comparing the inverse standard error weighted average of the 12 monthly regressions to the corresponding annual regression.

The linear regression to calculate the emission rate in Equation 5 is based only on the data for the emission mass flow rate and electricity supply from Q_{ru} and is therefore not subject to the demand balance constraint. Therefore, there will always be 365 samples, although some of them may be zero for less frequently used sources. As this process provides a modeled emission rate for the plants that do not have emissions data, there is no reason to perform separate monthly regressions, and we perform a single regression to determine $\hat{\gamma}^{E}_{ruh}$ for each hour of the day.

Emissions Data Processing

To assemble the plant emission mass flow rate profiles, E_{phi}, and supply profiles, S_{phi}, we follow the estimation of emissions methodology described in the Emissions & Generation Resource Integrated Database (eGRID) 2018 Technical Support Document [24] using the 2019 Environmental Protection Agency (EPA) Air Markets Program Data (AMPD) [26] CO_2 and gross electricity generation measurements, and the monthly total net generation (accounts for electricity consumed on-site at the plants) and heat input values reported in the 2019 Form EIA-923 [27]. The equivalent CO_2 profiles for the individual plants are assembled by scaling the EPA AMPD CO_2 profiles to account for the methane contribution. Methane emissions are not included in the EPA AMPD and are therefore estimated using the eGRID CH_4 emission factors [24] for the fuel types used at each plant, along with the heat input for those fuels in Form EIA-923. The methane emissions are weighted by a factor of 25 [24] to determine the monthly scaling factor that is used to convert the CO_2 profiles to equivalent CO_2 profiles. The net generation profiles for the individual plants are calculated by scaling the gross generation profiles from the EPA AMPD with the reported monthly total net generation values in Form EIA-923. The emission mass flow rates for plants that utilize biomass or produce useful thermal output Combined Heat & Power (CHP) are corrected according to the described the eGRID practice [24]. The designation of a plant as biomass or CHP is based on the 2018 eGRID [12] data, as is the primary fuel designation, and the assignment of the power plant balancing authority (BA).

The hourly CO_2 data from the EPA AMPD were integrated and compared with monthly CO_2 estimates calculated from the eGRID CO_2 emission factors and monthly heat input values from Form EIA-923 to confirm the validity of the CO_2 data for each plant. Similarly, the hourly gross generation data from the EPA AMPD were integrated and compared directly to the monthly net generation values in Form EIA-923. Several defined outcomes resulted from these comparisons and are classified into the following cases:

1. CO_2 estimates agreed with integrated EPA AMPD CO_2 profiles on a month-by-month basis to within 10%, and Form EIA-923 net generation was between 90% and 100% of the integrated EPA AMPD gross generation profile.
2. CO_2 and generation values differed by more than 10% on a month-by-month basis, but the resulting emission rate for the whole year from the EPA AMPD was within 10% of the value calculated from the Form EIA-923 data.
3. CO_2 estimates agreed with CO_2 profiles within 10% on a month-by-month basis, but net generation was higher than the integrated gross generation.
4. Month-by-month comparisons were inconsistent, but an annual comparison of the CO_2 emissions and generation revealed that the values were within 10%.
5. EPA AMPD was missing gross generation data or CO_2 data.

In the Case 1 classification, the CO_2 profile was scaled on a month-by-month basis to produce an equivalent CO_2 profile, and the ratio of net generation to integrated gross generation was used on a month-by-month basis to scale the gross generation and create a net generation profile. Case 2 classification was usually associated with plants that produce a net generation that is less than 90% of gross generation, but this result was consistent with the Form EIA-923 data, and therefore the plant could be treated the same way as Case 1.

The most common reason for the data to fall under the Case 3 classification was a generating unit that was not reported in the EPA AMPD, often due to cogeneration which, in many cases, provides extra generation without additional emissions. By subtracting this portion from the total monthly net generation for comparison purposes, the situation would often convert into Case 1 or 2. As the exact time variation of the missing generation was unknown, a constant net generation value (and equivalent CO_2 estimate if emissions were associated with the extra generation and were not included in the EPA AMPD) was recorded for each month based on the Form EIA-923 values. However, we included the contribution in the hourly profiles by scaling the CO_2 and gross generation profiles with factors that included the missing equivalent emissions and net generation thereby assuming that the time variation of the missing emissions and generation followed the same profile as the other emissions and generation.

Case 4 classification was common for gas turbine plants and indicated that the reported monthly data in Form EIA-923 may have been distributed over the year with an assumed annual profile. The Case 4 CO_2 and gross generation profiles were scaled with the annual scaling factors instead of monthly scaling factors to produce equivalent CO_2 and net generation hourly profiles. In Case 5 situations when gross generation data was missing, a net generation hourly profile was created using the equivalent CO_2 hourly profile and the annual plant emission rate calculated from the available EPA AMPD CO_2

FIGURE 4 2019 CISO natural gas source emission rate.

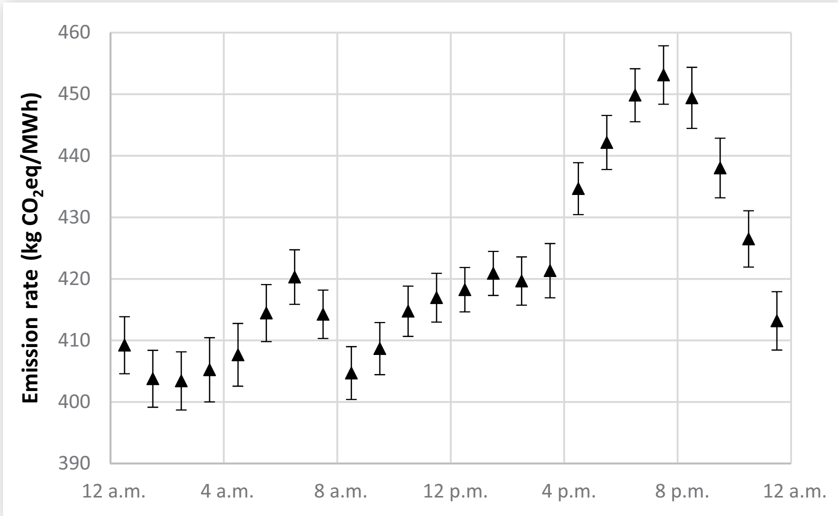

and the Form EIA-923 net generation. Similarly, in Case 5 situations where the EPA AMPD CO_2 data was missing, the hourly net generation profile and the annual plant emission rate based on the Form EIA-923 equivalent CO_2 estimates and net generation were combined to create the equivalent CO_2 profile. Note that the Case 5 profiles will always show a constant emission rate for the plant but will contribute time-varying CO_2 and net generation profiles to the combined plant emission rate profiles that we will use in this work.

Occasionally, individual months of the EPA AMPD were inconsistent with the remainder of the data and were recorded as constant monthly values based on the Form EIA-923 estimates instead of using the EPA AMPD profiles, but this was relatively uncommon. Exceptions were made for months with low or negative net generation as the 10% comparison thresholds were not relevant under those conditions. At the end of the data review process, each plant that was not rejected from consideration was assigned hourly equivalent CO_2 emissions and net generation profiles, in some cases calculated with assumptions of a constant emission rate or missing generation/emissions that matched the time profile of the other generation, along with a set of monthly constant values for inconsistent generation/emissions which were not utilized for the analysis in this work.

As an example, we consider the 83 natural gas plants in the 2019 EPA AMPD that were accepted after data review and were assigned to the California Independent System Operator (CISO or CAISO) BA region. Linear regression of the combined equivalent CO_2 with respect to combined net generation (supply) provides the emission rate $\hat{\gamma}^{E}_{ruh}$. Figure 4 shows this emission rate profile along with 95% confidence intervals. The fraction of the reported 2019 CISO average total natural gas generation [28] that is considered in the emission rate calculation ranges between 73% and 85% as shown in Figure

FIGURE 5 2019 CISO natural gas source average supply comparison.

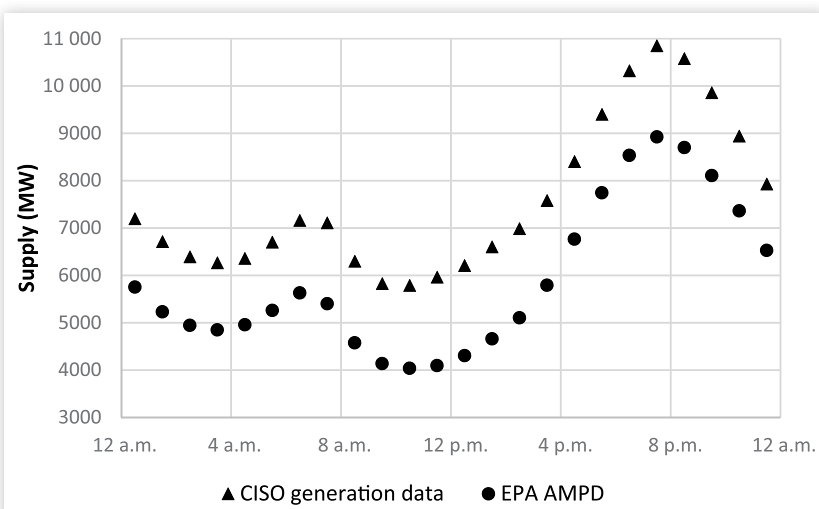

5, indicating that the calculated emission rate profile in Figure 4 is representative of a substantial portion of the natural gas electricity supply in the CISO region. The average EPA AMPD net generation profile also follows the average generation data time dependency closely, indicating that the 83 plants are the ones that are adjusting over the day to changes in the need for natural gas electricity. The emission rate in Figure 4 is highest during peak hours as less efficient plants are brought online to meet demand.

In most cases, the emissions data for coal and natural gas in the EPA AMPD accounted for over 90% of the generation reported in the electricity supply data for any given region. Therefore, the modeled emission rate profiles were a minor contribution to the total emission mass flow rate and the marginal emission rate. Data for oil plants was far less complete and the modeled emission rate was more important. However, the contribution to the marginal emission rate from oil was usually less than 1% in most regions.

CISO Grid Data

California announced a goal of 100% zero tailpipe emissions vehicles by 2035 [29]. The challenges to California's electrical grid supporting a 100% BEV fleet beyond 2035 are significant. In 2018 California's in-state electricity generation was 195 TWh with a further 90 TWh imported from other U.S. states, Canada, or Mexico, yielding a total electricity need of 285 TWh. A total of 32.3% of in-state electricity was generated from renewable sources: solar (14.0%), small hydro (2.2%), wind (7.2%), geothermal (5.9%), and biomass (3.0%) [30].

California's transportation energy requirements for 2018 were 929 TWh, where 98.3% of that energy came from petroleum products [31]. There are several end uses for petroleum: aviation gasoline, distillate fuel oil (diesel and biodiesel blends), hydrocarbon gas liquid (propane), jet fuel, lubricants, motor gasoline, and residual fuel oil. In 2018, 56.6% of petroleum was used for motor gasoline [31]. Thus, 517 TWh of the gasoline chemical energy would need to be replaced by electricity for the future EV fleet. However, the well-to-wheel efficiency of a BEV is two-to-three times higher than a conventional ICEV [32, 33, 34]. Assuming an efficiency multiplier of 2.5 yields 207 TWh of additional electrical grid capacity that will be required to support the potential 100% EV passenger car fleet, this represents a 73% increase in total electricity generation compared to 2018, but more significantly a 429% increase in renewable electricity generation if the use of EVs is to conform with "zero-emission" targets. The largest net output from a single solar source in 2018 was 1.34 TWh from the 7.3 mi^2 Topaz Solar Farm located in San Luis Obispo County [35]. To supply a 100% EV fleet with renewable energy would require 155 additional sites to meet the future vehicle charging needs with solar arrays. The cost to make these new sites adjusted for inflation in 2020 would be around $434 billion USD while approximately 1132 mi^2 (2932 km^2) of land would be required (over twice the land area of the city of Los Angeles).

Renewable electricity can substantially lower the emissions associated with the total generated electricity, but supply is typically unsteady due to the stochastic nature of solar and wind availability. California's grid utilizes photovoltaic (PV) solar arrays during the day, and natural gas in the morning and evening to buffer the deficit from reduced solar potential (see Figure 6). Therefore, the time of day when BEVs and PHEVs are charged, along with several other factors, will play a role in determining the type of electricity that is available and used, and the GHG emissions produced.

As solar electricity is not readily available at all times of a day, the solution to a California fleet with increasing levels of BEVs is more complex than just adding solar arrays to the grid. Technologies such as vehicle-to-grid (V2G) and vehicle-to-home (V2H) have the potential to allow solar electricity to supply a larger portion of the required increase in electricity

FIGURE 6 California electricity generation (03/03/2020). Data taken from Ref. [28].

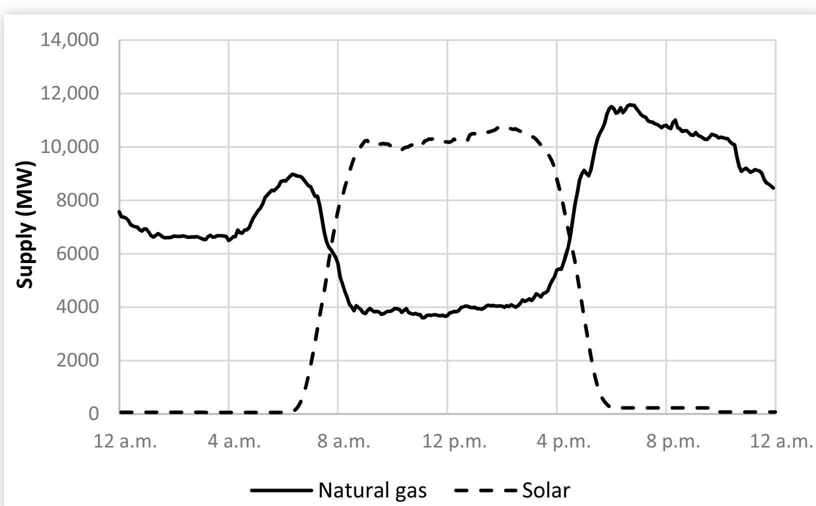

FIGURE 7 CISO September 2019 4 a.m. supply data.

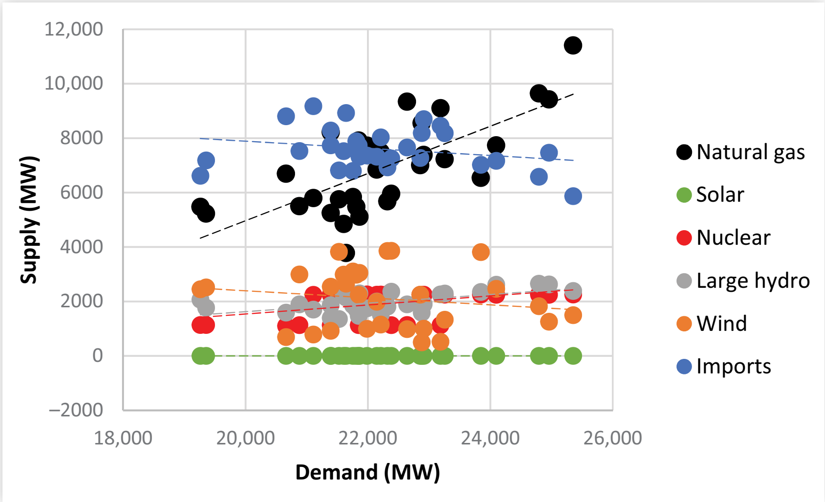

Data taken from Ref. [28]. © Convergent Science, Inc.; Southwest Research Institute; Scott Powers; Felix Leach

demand, but it is unknown how quickly V2G and V2H compatible homes and vehicles will become mainstream. Storing electricity in batteries will require further investment in infrastructure, in addition to the CO_2 footprint associated with battery production. Although batteries are the cheapest form of energy storage now, there are other methods of energy storage including ammonia, chemical, compressed air, flywheel, hydrogen, magnetic, pumped hydro, thermal, and thermochemical [36] that may also prove useful.

Besides solar, other non-emitting electricity sources will be unable to contribute in California as there are no plans for additional nuclear power plants, hydropower cannot be scaled and more recently has, in fact, been reduced due to drought conditions, and wind farm capacity has remained constant for the past eight years. It is likely that much of the additional electricity required for the larger BEV fleet will have to come from fossil fuel-based sources. A detailed study of high BEV adoption impacts on the Western U.S. grid including light-duty, medium-duty, and heavy-duty vehicles concluded that the additional generation required for charging would most likely come from natural gas power plants [21], although seasonal renewable curtailment reductions would also occur.

Figures 7 and 8 show September 2019 supply versus total demand data from the CISO website [28] for 12 electricity sources: natural gas, imports, large hydro, wind, solar, nuclear, coal, battery, geothermal, biomass, biogas, and small hydro, at 4 a.m. when the demand is lowest. Similarly, Figures 9 and 10 show the data at 2 p.m. when the solar electricity supply is near its peak, and Figures 11 and 12 show the data at 6 p.m. when the demand is relatively high. The figures include monthly regression trendlines for each electricity source. Each point represents the reported source value at the same time

FIGURE 8 CISO September 2019 4 a.m. supply data.

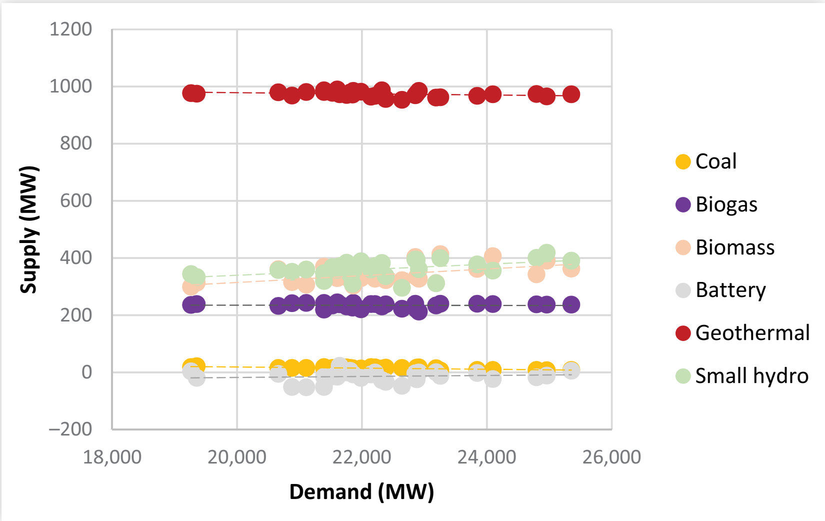

Data taken from Ref. [28]. © Convergent Science, Inc.; Southwest Research Institute; Scott Powers; Felix Leach

FIGURE 9 CISO September 2019 2 p.m. supply data.

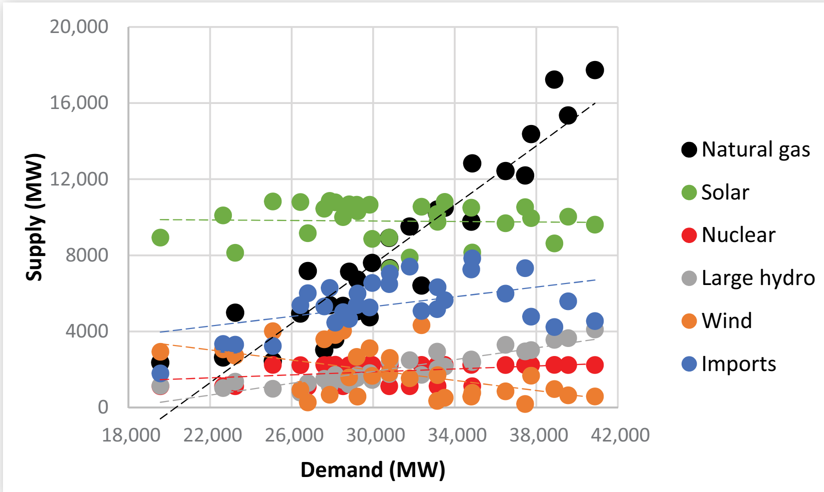

Data taken from Ref. [28]. © Convergent Science, Inc.; Southwest Research Institute; Scott Powers; Felix Leach

of day, averaged over a 5-minute interval, on a different day of the month, and is an aggregation of power plants using the source. Except for the 2 p.m. time, when solar supply is high, most of the load is carried by natural gas and imports. What is more important are the slopes of the trendlines as they indicate how the individual source contributions are used to provide for an extra load that is added to the grid at that time of day. The steepest slope is usually associated with natural gas indicating that it is used more than any other source to meet changes in demand, i.e., it is the primary marginal source. Large hydro can load follow and is used the most to meet demand changes around the 6 p.m. time when demand is approaching a maximum and the trendline has a positive slope. Many of the other sources are invariant with respect to demand or have relatively low magnitude slopes of their trendlines indicating that they do not act as marginal sources of electricity at that time. Figure 9 demonstrates that, even when the supply of solar electricity is high, it does not produce more or less electricity in response to demand changes.

The data in Figures 7 through 12 demonstrate why sources are placed into the non-marginal category. Except for large hydro, none of the other non-emitting sources demonstrates any consistent trend with demand and cannot affect the marginal emission rate. However, these non-emitting sources do reduce the marginal demand that must be met by the marginal sources, thereby minimizing the total emissions. California has large solar resources and curtailment is sometimes required due to excess solar electricity. However, additional technology development and/or demand management are required to allow solar to directly influence the marginal emission rate.

FIGURE 10 CISO September 2019 2 p.m. supply data.

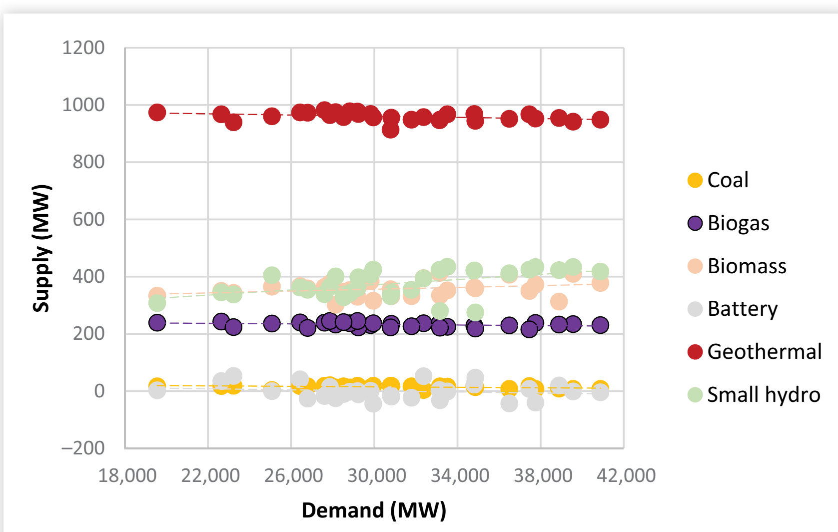

Data taken from Ref. [28]. © Convergent Science, Inc.; Southwest Research Institute; Scott Powers; Felix Leach

FIGURE 11 CISO September 2019 6 p.m. supply data.

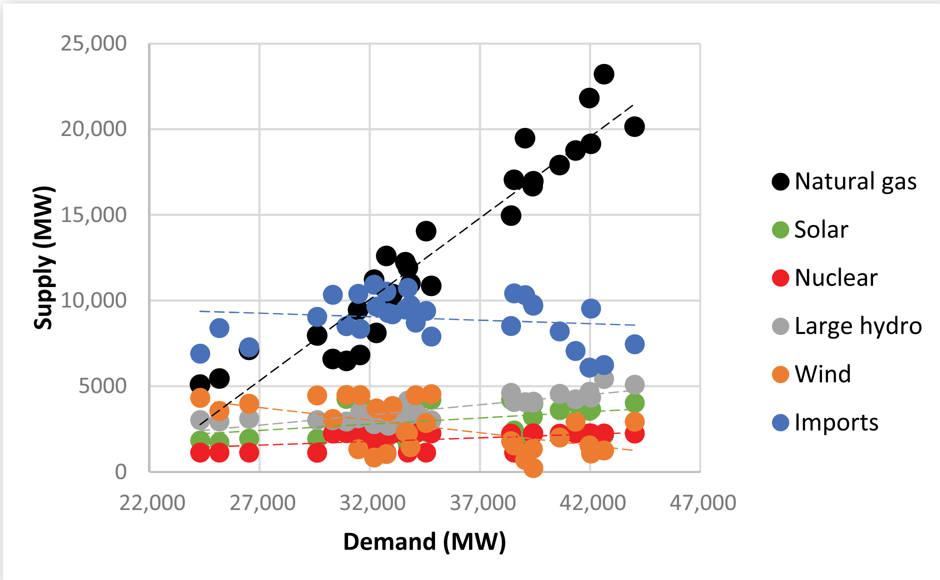

Data taken from Ref. [28]. © Convergent Science, Inc.; Southwest Research Institute; Scott Powers; Felix Leach

The 2019 CISO 8 a.m. annual supply data for solar, wind, nuclear, and natural gas are shown in Figure 13. The different symbols are associated with different months, and the plots also include individual monthly trendlines. The annual regression procedure described previously fits trendlines to the data with a single slope, but different intercepts. There is no consistent trend with demand for solar, wind, and nuclear sources, and therefore, the slope value from the annual regression will most likely be close to zero and the value will not be statistically significant. The data for solar and wind in Figure 13(a) and (b) show that there is substantial variance which is not accounted for by the linear trendlines. This results in low R^2 values for the associated monthly and annual regressions. Figure 13(c) shows that the nuclear source in the CISO region operated overwhelmingly near two discrete electricity generation levels across the entire demand range. While most of the monthly trendlines have slopes very close to zero, the months where the reactors were powered down or up show poor regression quality and have non-zero slopes which are not representative of the true nuclear supply demand response. It is for this reason that nuclear is assigned to the non-marginal category by default. Figure 13(d) for natural gas demonstrates the demand response of a marginal source. Many of the months have trendlines with similar positive slopes, and the

FIGURE 12 CISO September 2019 6 p.m. supply data.

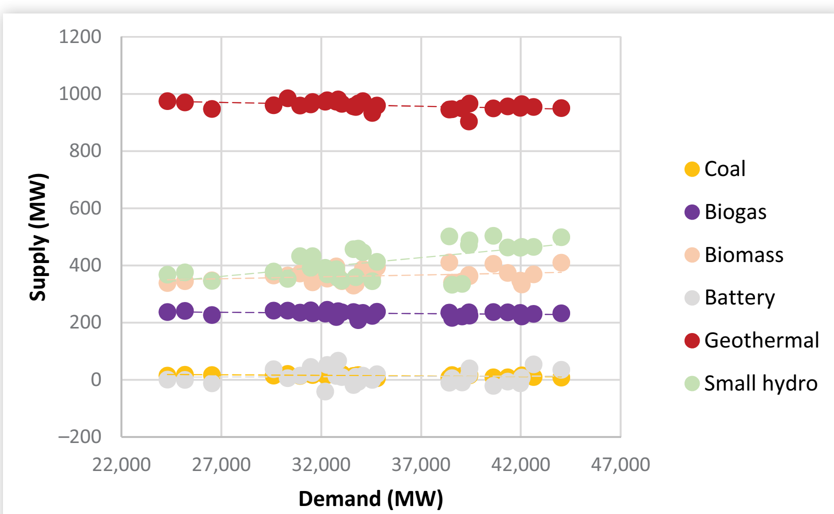

Data taken from Ref. [28]. © Convergent Science, Inc.; Southwest Research Institute; Scott Powers; Felix Leach

FIGURE 13 CISO 2019 8 a.m. annual regression data by month (symbols with trendlines). (a) Solar; (b) Wind; (c) Nuclear; (d) Natural gas.

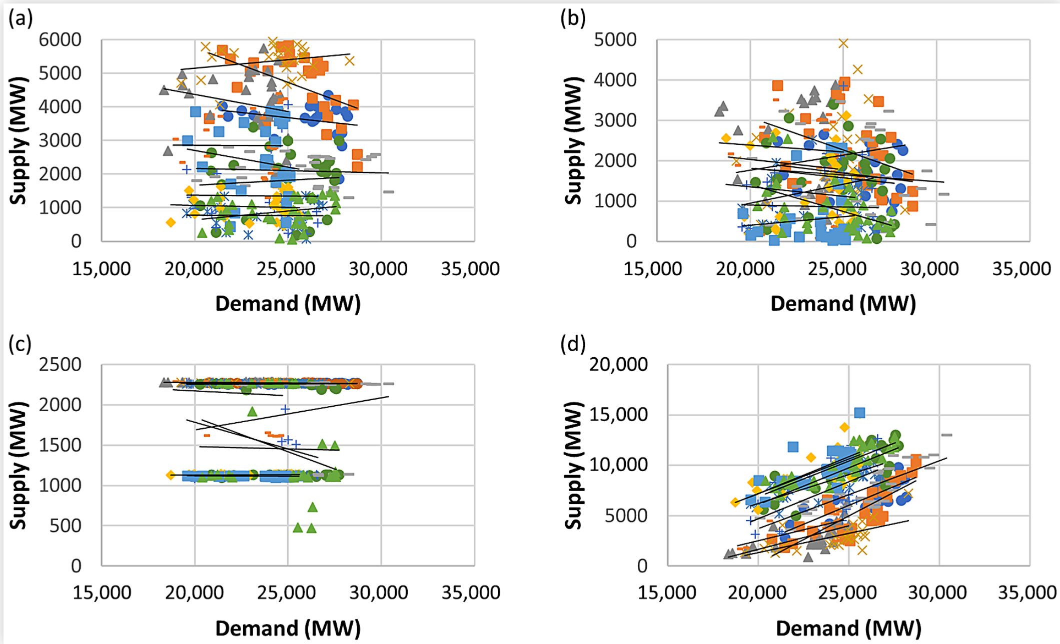

annual regression procedure will produce a slope with a magnitude close to one, indicating that natural gas is the dominant marginal source at this time of day.

It is important to interpret the assignment of nuclear (at all times) and solar and wind (depending on statistical significance) to the non-marginal category correctly. The data indicates that it is unlikely that a load added to the CISO grid will be met by any of these sources because they do not consistently increase with demand. It is plausible that a load added to the grid will be timed such that a nuclear reactor is generating a slightly higher power level, or when extra wind or solar electricity becomes available due to favorable conditions. However, short-term fluctuations may just as easily lead those sources to diminish. Considering the symmetry in the addition and removal of a load from the grid, it becomes clear that, because these sources do not respond to demand, the addition or removal of loads from the grid will not directly lead to a change in those sources. Instead, a demand change will be met by a change in some combination of marginal sources, and depending on their makeup, the total grid emission rate will change accordingly. Note that our analysis does not rule out solar and wind from acting as marginal sources, and in certain regions and certain times of day, these sources will affect the marginal emission rate directly.

The total reported CISO demand and fraction of the demand met by sources with at least 1% of the total demand are shown in Table 1 for both 2019 and 2020. The largest change between the two years was the reduction in large hydro in 2020 which was compensated for with natural gas and imports. This highlights the finite capacity of hydro-generated electricity, although our analysis does not preclude it from acting as a marginal source on this basis.

The importance of imports to the CISO region is evident in Table 1. Due to high demand in California, imports from the Southwest and Pacific Northwest are required. A description of the composition of these imports is available on the California Energy Commission website [37]. In 2019, 10.34% of imports were coal, 11.55% were natural gas, 26.38% were unspecified, and the remainder were non-emitting sources. However, assigning an emissions intensity to these imports is more complex than assuming that the imports have a fixed source composition. If CISO imports hydroelectricity from another region and that region imports coal electricity from elsewhere to make up for the hydro that could have been used locally to meet demand, then the marginal emission rate for the load in the CISO region should reflect a contribution from the associated coal generation. This approach is consistent with the requirement that displacement of emissions to

TABLE 1 CISO annual grid data demand and fractional supply comparison.

	Demand (GWh)	Natural gas	Imports	Solar	Large hydro	Nuclear	Wind	Geothermal	Small hydro
2019	217.9	0.297	0.237	0.132	0.119	0.074	0.073	0.035	0.016
2020	217.6	0.339	0.259	0.140	0.065	0.075	0.076	0.036	0.009

another location should not be permitted when calculating the appropriate emission rate. Note that the reassignment of emissions responsibility only occurs if the associated imports are placed in the marginal category for the regions involved in the transfer. R^2 values for the regressions of imports are usually lower than for the emitting sources, indicating that at least some of the imports are scheduled in advance and not strictly a response to an increase in total demand.

The frequent exchange of electricity between the different regions requires that the emission rate includes the effect of imports. Table 1 provides the aggregate electricity imports for the CISO region, but since each region generates electricity with a different emissions intensity, the imports and exports between regions must be considered as individual interchanges between regions, rather than in aggregate. We now present a coupled analysis of the electric grid in the contiguous U.S. to estimate the marginal emission rates accounting for the coupling between geographic regions.

U.S. Grid Analysis

The electric grid for the contiguous United States is made up of several smaller grids that are grouped into three major interconnections which operate relatively independently with high-voltage DC connections between them. The approximate geographic regions covered by these interconnections are shown in Figure 14 [38]. The Eastern Interconnection includes most of the country from the Great Plains to the Atlantic Ocean, the Western Interconnection covers everything west of the Great Plains states to the Pacific Ocean, and the Texas Interconnection covers almost all of the state of Texas. Some portions of the U.S. grid are also connected to grids in Canada and Mexico. The electricity supply in each interconnection is managed by the BAs that are responsible for controlling the generation of electricity within smaller regions and exchanging electricity with neighboring BAs to meet demand and maintain the stability of the grid. The complete list of BAs and their acronyms can be found on the EIA website [39]. While there is a nominal geographic region associated with many of the BAs, there are areas with substantial overlap of BA coverage. For example, Washington and Oregon combined have 11 BAs, California has five, and Arizona has seven. Because of this organizational structure, it makes sense to analyze the U.S. grid based on BAs and then apply the results of the analysis to the appropriate states keeping in mind that individual states may be served by multiple BAs. The circles in Figure 14 show the approximate locations where U.S. BAs operate, along with the neighboring BAs in Canada and Mexico.

Hourly data for the 68 U.S. BAs are available on the EIA website [40]. The data includes demand, total generation, generation by electricity source, total interchange with all connected BAs, and individual interchanges with other BAs, which are reported in real time to the EIA. The source categories are coal, natural gas, nuclear, oil, hydro, solar, wind, other, and unknown. Many spurious values are automatically corrected in the data to produce adjusted values that we will use here for our analysis. In addition to these corrections, the 2019 data were corrected in other ways by the present authors based on the investigation of large imbalances in the following: demand versus supply, sum of individual source supplies versus total supply, total interchange versus the sum of interchanges, and individual interchanges as reported on both sides. Phase shifted data are relatively easy to identify and

FIGURE 14 Contiguous U.S. grid interconnections and BA (circles) approximate locations.

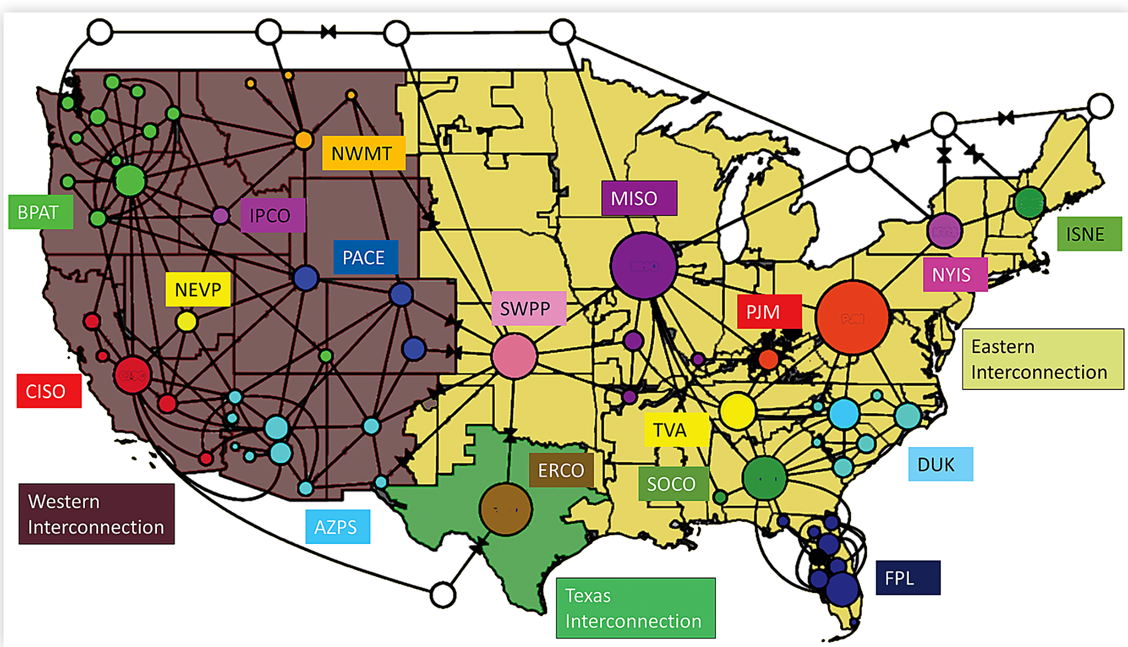

Adapted from Ref. [38]. Source: U.S. Energy Information Administration (Oct 2008) correct for when generation consistently leads demand, or when individual interchange data are reported in local time instead of UTC time. Missing generation can also be identified in many cases by noting the profile of the missing generation. Because of their unique profiles in time, errors in nuclear and solar generation data can easily be corrected. The EPA AMPD was also used to identify missing generation data with a high degree of confidence in cases where a near-perfect correlation was obtained between the hourly net generation profiles from individual plants and the missing data. Several power plants were identified as having joint ownership between Bas, which allowed us to identify the source of the coal generation in a geographic region without coal plants and to correct a nuclear source that was reported twice. The combined net generation data in Form EIA-923 [27] for all plants in the United States is also useful to help identify the source of any missing generation.

The data rejection methodology required that the imbalance between demand, imports/exports, and total supply was less than a specified percentage of total demand and that the difference between the reported total supply and the sum of the individual reported electricity source supplies was within a specified percentage of the total supply. There was no data rejection threshold applied to the balance between the total interchange and the sum of the individual interchanges. However, when individual BAs disagreed significantly on the interchange, we selected the value from the BA which demonstrated a better overall balance in their other data. In most cases, these discrepancies can be identified as missing generation or are relatively small in magnitude. The different BAs show a wide range in terms of quality of the reported data, and some were much easier to correct than others. After the data cleaning, most of the imbalances were reduced to less than 4%, which makes the dataset useful for regression purposes.

Due to the tightly coupled nature of some of the BAs, both geographical and resource wise, it was advantageous to group the individual BAs together. However, we aimed to maintain geographic granularity of the data as the supply and management of the electricity sources can be very different between BAs. Therefore, the BA groups are not compiled to match total demand or generation magnitudes between groups, but rather to facilitate regional analysis including interchanges between them. The BA groups and the associated individual BAs within them are listed in Appendix A along with the final applied data rejection threshold and the resulting minimum and maximum sample sizes for the annual regressions performed for each hour of the day. The BAs associated with each BA group are shown in Figure 14 as circles of the same color.

For each BA group, the contributions to demand and supply and the individual sources from the group members were added together, and the imports/exports to adjacent neighboring BA groups were calculated as the sum of the interchanges between all the BA group members with any members of the adjacent BA groups. Imports into a BA group from other BA groups were each treated separately since the emission rate for the imports will be different depending on the BA group of origination. Zivin et al. [41] recognized the difficulty associated with accounting for imports and exports of electricity and chose to perform their marginal emission rate analysis at the interconnection level since the interconnections are relatively independent and imports and exports between them could be ignored.

The nuclear source is always placed in the non-marginal category, and the remaining sources and imports are evaluated for statistically significant total demand response to determine their classification for marginal emission rate determination. The emission rate for an import in a BA comes from the regressions in the BA that provides the import. As the regressions in the neighboring BA may also include imports from other BAs, the coupled system in Equation 15 must be solved for all BA groups to determine the final marginal emission rates. This coupled system was assembled after the $\hat{\beta}^{Y}_{rh}$ and $\hat{\beta}^{T}_{rqh}$ values were determined for each region and iterated until convergence.

The emissions data from individual plants in the EPA AMPD that were assigned to a BA within a BA group were combined by source as discussed previously. In some cases, the combined net generation profiles from the EPA AMPD exceeded the combined source generation data from the EIA. It is not always straightforward to identify exactly which BA is reporting the generation data for an individual plant as there are many situations where a plant owned by an entity associated with one BA is located geographically in a region managed by another BA. Therefore, we defined the set Q_{ru} for emissions data processing as the plants that produced the highest correlation coefficient and minimum root mean square error between the EPA AMPD net generation profile and the combined EIA source generation profile, and the calculations of the correlation coefficient and root mean square error excluded the data points that did not meet the required source balance criteria. In all cases, the emission rate, $\hat{\gamma}^{E}_{ruh}$, for the plants in set $Q^{'}_{ru}$ was modeled using all plants assigned to the BA group.

Table 2 presents summary data from the analysis. The source dataset includes a total of 4021.5 TWh of demand data which is met by the combination of generation within each BA group and imports from neighboring BA groups. After applying the data rejection thresholds in Appendix A, 3587.8 TWh of the total data were used for regression purposes. The average (over all 24 annual regressions for each BA group) statistically significant marginal emission rate (lower bound) and emitting source marginal emission rate (upper bound) are shown in Table 2 for the local generation (weighted $\hat{\beta}^{Y}_{rh}$) and the total including imports. The average mix emission rates based on the same data are also presented for each BA group in Table 2. In most regions, the average mix emission rate represents a dramatic underprediction of the lower bound for the marginal emission rate. Weighting the averages from each BA group by demand produces a 2019 U.S. marginal emission rate of 587.2 kg CO_2eq/MWh for the lower bound and 654.1 kg CO_2eq/MWh for the upper bound, which are 43.2% and 59.5% higher than the corresponding U.S. average mix emission rate, respectively.

The top three marginal sources, averaged over all 24 annual regressions, for each BA group based on the statistically significant marginal source selection procedure are also

TABLE 2 2019 U.S. electricity grid analysis summary.

BA group	Total demand (TWh)	Useful demand (TWh)	Average marginal emission rate (kg CO_2eq/MWh) lower/upper bound	Generation-only average marginal emission rate (kg CO_2eq/MWh) lower/upper bound	Generation-only average mix emission rate (kg CO_2eq/MWh)	Primary marginal sources (statistically significant marginal source selection)
AZPS	104.45	85.09	543.7/567.2	524.7/539.0	456	Gas (63.4%), coal (18.3%), PACE (12.6%)
BPAT	162.34	142.64	91.9/584.0	93.4/691.0	186	Hydro (55.2%), wind (21.2%), BCHA (7.5%)
CISO	267.83	232.05	396.3/468.6	411.1/446.5	196	Gas (72.6%), BPAT (9.0%), AZPS (7.9%)
DUK	223.01	185.88	676.5/786.1	677.3/792.8	299	Coal (54.2%), gas (27.4%), hydro (10.4%)
ERCO	383.66	383.32	508.4/528.9	508.3/527.9	401	Gas (74.3%), coal (20.4%), wind (5.0%)
FPL	241.37	202.54	453.7/472.7	439.5/457.7	382	Gas (80.8%), coal (8.6%), SOCO (5.3%)
IPCO	19.49	19.31	635.1/751.0	610.3/771.6	210	PACE (59.2%), coal (17.1%), gas (11.4%)
ISNE	118.29	118.18	408.5/432.6	409.4/432.5	216	Gas (86.4%), coal (3.9%), hydro (3.5%)
MISO	673.64	620.06	749.1/766.5	749.3/766.6	560	Coal (51.7%), gas (39.9%), oil (6.8%)
NEVP	32.27	31.35	513.4/535.0	528.3/530.5	396	Gas (58.9%), CISO (20.3%), coal (11.3%)
NWMT	13.33	12.85	820.5/1018.7	824.1/1025.2	690	Coal (80.8%), wind (19.4%)
NYIS	155.82	155.22	477.5/519.6	468.9/516.7	174	Gas (66.4%), PJM (15.4%), HQT (5.9%)
PACE	119.04	111.90	673.3/755.0	758.0/777.0	690	Coal (47.2%), cas (32.0%), BPAT (11.3%)
PJM	835.02	721.75	689.5/724.4	690.7/725.2	395	Gas (48.0%), coal (46.2%), hydro (2.7%)
SOCO	243.15	242.34	686.8/703.6	692.8/707.4	454	Gas (54.5%), coal (37.3%), TVA (5.1%)
SWPP	269.50	210.59	523.5/762.2	521.7/762.1	492	Coal (38.2%), wind (36.4%), gas (24.0%)
TVA	159.33	112.76	597.2/640.8	576.5/622.0	313	Gas (51.0%), coal (29.7%), MISO (12.2%)

shown in Table 2. Some of the BA groups have marginal international imports, e.g., New York Independent System Operator (NYIS) and Bonneville Power Administration (BPAT), which were assumed to have zero marginal emission rates. In most of the BA groups, coal and natural gas are the primary marginal electricity sources with wind and hydro also playing substantial roles. The Arizona Public Service Company (AZPS) BA group demonstrates the scenario mentioned previously where exports of lower marginal emission rate electricity to the CISO BA group occur simultaneously with imports of higher marginal emission rate electricity from the PacificCorp East (PACE) BA group, which leads to a 3.6% increase in marginal emission rate when imports are included versus the local generation marginal emission rate (statistically significant marginal). There have recently been several coal plant closures in the AZPS BA group region, and the generation will need to be replaced with local natural gas or non-emitting generation, or imports from other BA groups. The imports into the PACE BA group from the BPAT BA group lead to a reduction in the marginal emission rate including imports as compared to the generation marginal emission rate. The CISO BA group also shows a drop in the marginal emission rate including imports due to low marginal emission rate imports from the BPAT BA group for the statistically significant marginal source selection. However, the emitting source marginal source selection emission rate for CISO is higher than the generation value because the imports from AZPS and BPAT have a higher emissions intensity than the CISO generation for that selection methodology. Many of the BA groups in Table 2 show a difference between marginal emission rates of less than 10% for the two different source selection methodologies. The BA groups with substantial contributions from marginal wind and hydro sources show much larger discrepancies between the different marginal source selection methodologies, as expected.

The hourly marginal emission rates and associated standard errors for all BA groups in the local time zone are presented in Appendix B for the statistically significant marginal source selection methodology, where the hour indicates that all data used for the calculation were average values over the prior 60 minutes, e.g., hour 1 is based on data between 12 a.m. and 1 a.m. and hour 24 is based on data between 11 p.m. and 12 a.m. The standard errors were computed by combining the standard error from the regressions of the emissions for the local generation with the corresponding weighted standard errors from all other BA groups that provided marginal imports to the BA group in question, ignoring any correlation between separate BA group emission rate profiles as they were obtained from regressions with respect to relatively (although not completely) independent demand variables. The standard errors are larger as a percentage of the hourly marginal emission rate for the BA groups with significant wind energy in the marginal mix. Wind contributes directly to the Electric Reliability Council of Texas, Inc. (ERCO) BA group as a marginal source only in the 11 a.m. to 7 p.m. time period, and Appendix B shows that the marginal emission rate drops by around 10% during these hours, but the standard error increases substantially. In the Southwest Power Pool (SWPP) BA group, wind makes the largest contribution to the marginal emission rate of any of the BA groups, and the standard errors are also the largest.

The marginal emission rate profiles are shown in Figure 15 for the BPAT, CISO, Midcontinent Independent System Operator, Inc. (MISO), and SWPP BA groups. These four represent some of the larger demand BA groups, have different marginal mix compositions, and span the range of average marginal emission rates in Table 2. The MISO profile is relatively flat over the course of the day, while the SWPP profile shows substantial hour-to-hour variation due to fluctuations of the wind source. During the 7 a.m. to 9 a.m. time window, the wind falls out of the marginal source category for SWPP and the marginal emission rate is virtually identical to the MISO marginal emission rate. The CISO profile shows lower marginal emission rates between 5 a.m. and 5 p.m. due to the contributions of local hydro generation and imports from BPAT which make up approximately 20% of the marginal mix during that time window. While solar provides a substantial amount of electricity for CISO during daylight hours, it does not affect the marginal emission rate directly but instead serves to reduce the marginal demand. Finally, the BPAT profile in Figure 16 shows an increase from the overnight hours, where wind and hydro dominate the marginal mix, to midday due to coal and gas marginal sources. However, the wind source remains as large a contribution to the marginal as either gas or coal at nearly all hours of the day, and hydro is consistently the strongest marginal source, keeping the marginal emission rate relatively low compared to all other BA groups.

The coefficients of determination for the emission mass flow rate regressions (see Equation 12) are shown in Figure 16 (closed symbols) for the same four BA groups. The MISO marginal mix is dominated by local generation from emitting sources and has the highest R^2 values as a result. The CISO marginal mix is mostly gas, but also includes substantial contributions from hydro and imports. It is the imports that lead to the reduction in the R^2 values in comparison to MISO as the regressions of the hydro source, with respect to marginal demand, typically produce high R^2 values for the CISO BA group. The BPAT and SWPP marginal mixes include wind, which further reduces the R^2 values of the emission mass flow rate regressions for these BA groups in Figure 16. Effectively, the wind is dictating how much the emitting sources should respond to demand. In fact, the BPAT region actively coordinates supply from natural gas plants and a nuclear plant to balance the supply of wind and hydro with demand [42, 43]. The R^2 values for regression of the wind source versus marginal demand for BPAT and SWPP are also shown in Figure 16 (open symbols), which indicate that the variance in the wind source is not accounted for by changes in the marginal demand as expected. The large wind contribution to the SWPP marginal mix is evident in the relatively low R^2 values for the emission mass flow rate regressions and leads to much larger uncertainty for the SWPP BA group than any other BA group. The highest R^2 values for the SWPP emission mass flow rate regressions in Figure 16 occur at those times of day when the wind is the smallest fraction of the total generation (12 p.m. to 9 p.m.).

The uncertainty in the supply of some of the non-emitting sources leads to uncertainty in the marginal emission rate predictions when they are considered as marginal sources. While all sources are subject to finite capacity, the limits for the emitting sources are approached far less frequently. Ideally, non-emitting sources are always utilized at their maximum available capacity to reduce the total grid emissions as much as possible, but this prevents them from acting as marginal

FIGURE 15 Hourly marginal emission rates for BPAT, CISO, MISO, and SWPP BA groups.

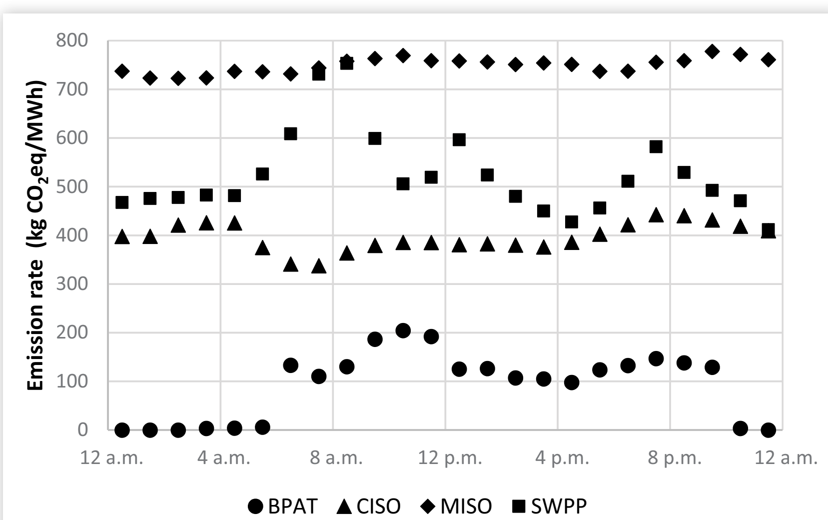

FIGURE 16 2019 BA group emission mass flow rate regression coefficients of determination.

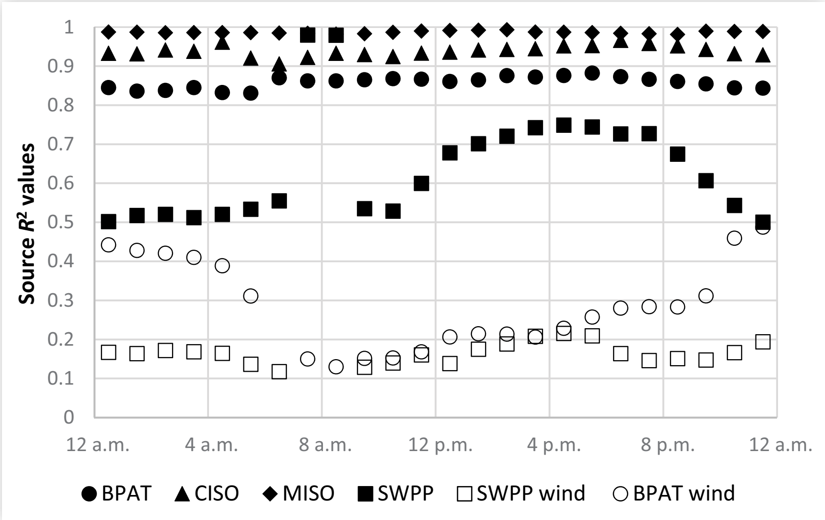

sources and leads to emitting sources being used in the marginal mix. Therefore, we also present the emitting source marginal emission rates in Appendix C as an upper bound on the marginal emission rate. The 95% confidence interval half-widths for all BA groups are less than 10% of the marginal emission rate and, for many BA groups, are less than 5% of the marginal emission rate. By way of comparison, the statistically significant marginal source selection methodology produced 95% confidence interval half-widths as high as 30% for the marginal emission rate.

The marginal emission rates calculated here are strictly valid only for the addition or removal of a load at the 2019 demand and supply conditions and should be used with some caution far from those conditions. However, the data can also be used to assess the change in marginal emission rate as marginal demand drops. Table 3 shows that by removing the highest marginal demand samples (top 10%) from the regressions, the average marginal demand is reduced by between 107 MW and 2507 MW, depending on the BA group, but that there is very little difference between the original statistically significant methodology average marginal emission rate and the corresponding reduced demand average marginal emission rate. Except for hydro (which cannot be scaled up) and some wind resources (depending on how they are managed), most renewable electricity generation does not act as a marginal source of electricity and, therefore, serves only to reduce the marginal demand. The minimal marginal emission rate changes in Table 3 indicate that there was not a substantial bias toward higher carbon intensity generation at higher marginal demand levels. Therefore, depending on grid management, the addition of renewable generation which decreases marginal demand will not lead to a proportional reduction in the marginal emission rate. This complexity of the electricity supply process is ignored entirely by average mix emission rate calculations and can only be evaluated through the analysis of grid data.

All loads should be considered marginal in the sense that if any of them are individually removed from the grid, the resulting emissions reduction can be calculated from the marginal emission rate. For assigning emissions to larger loads of interest, the marginal emission rate calculation should be checked for demand sensitivity as shown in Table 3. Unless the supply and demand changes are such that a previously unutilized source must now be utilized, currently utilized

TABLE 3 Statistically significant marginal emission rate demand reduction summary.

BA Group	Average marginal demand reduction (MW)	Average marginal emission rate (kg CO_2eq/MWh)	Reduced demand average marginal emission rate (kg CO_2eq/MWh)
AZPS	467.4	543.7	546.0
BPAT	472.6	91.9	101.2
CISO	902.3	396.3	384.4
DUK	771.8	676.5	652.8
ERCO	1495.6	508.4	508.0
FPL	861.3	453.7	443.8
IPCO	148.9	635.1	613.7
ISNE	376.3	408.5	401.5
MISO	1903.2	749.1	750.3
NEVP	163.0	513.4	504.0
NWMT	107.2	820.5	909.4
NYIS	512.6	477.5	451.3
PACE	411.1	673.3	691.6
PJM	2506.9	689.5	668.7
SOCO	880.0	686.8	672.8
SWPP	801.2	523.5	492.5
TVA	588.0	597.2	596.9

sources are operated in substantially different ways, a source can be abandoned, or a previously non-marginal source is operated to allow it to respond to demand directly, the marginal emission rate will be relatively stable, and it is appropriate to apply it for emissions calculations. Renewable electricity generation eventually will reach levels in more U.S. regions where curtailment is required, which will allow it to act as a marginal source and directly impact the marginal emission rate.

As the United States considers a 50% light-duty BEV sales target by 2030 to reduce CO_2 emission, those sales should come in regions of the country where the marginal emission rate is low enough to provide an emissions benefit for BEVs over alternatives. Adding 8.5 million BEVs to the U.S. fleet in an individual year would require approximately 12 GW of additional overnight generation capacity (assuming 75 kWh packs charging once per week at night for 8 hours) to come from a combination of sources that produce less CO_2 than the combustion process in a hybrid vehicle. In the next section, we will consider which regional grids have a marginal emission rate that currently justifies increased BEV adoption and which grids need further decarbonization before aggressively pursuing the transition to all-electric fleets.

Vehicle CO_2 Emissions Comparison Methodology

A large number of factors affect the total GHGs and other environmental impacts associated with the production, operation, and eventual disposal of a vehicle [44]. In reporting comparisons between vehicle types, it is important that consistent contributions are included for all vehicles. However, to make the comparison useful to consumers, it is preferable to focus on only the largest contributions that can be easily communicated, allowing them to reach their own conclusions.

Fuel Consumption

The U.S. Department of Energy provides fuel economy/consumption data for vehicles on their website [45]. In the case of BEVs, the fuel consumption is reported in kilowatt-hour per 100 miles and includes charging losses. ICEV and FHEV fuel economy is reported in miles per gallon. For PHEVs, fuel economy values are reported for the conventional fuel, e.g., gasoline (charge-sustaining operation), in miles per gallon, and fuel consumption values are reported for charge-depleting operation in kilowatt-hour per 100 miles.

The fuel consumption and fuel economy values are based on the EPA-prescribed test cycles [46]. The EPA testing includes a city (Federal Test Procedure [FTP]) and highway test (Highway Fuel Economy Test [HWFET]), and three additional tests designed to make adjustments for aggressive driving (US06), and operation in hot (SC03) and cold (Cold FTP) weather with increased heating, ventilation, and air conditioning (HVAC) operation to provide consumers with more realistic estimates. However, the adjustments to the city and highway fuel consumption numbers for BEVs and PHEVs in charge-depleting operation are typically obtained by dividing the city or highway test fuel consumption values by 0.7. While this procedure may allow for comparison between individual BEVs and PHEVs, it is problematic when a vehicle with an adjusted fuel consumption value based on the additional tests is compared to a vehicle where a division by 0.7 was used. Therefore, we will account for real-world driving effects corrections for the BEVs and PHEVs in a different way and use a consistent methodology for the FHEVs and ICEVs to allow meaningful comparisons.

The American Automobile Association (AAA) published a report in 2019 [47] on the effect of ambient temperature and the associated increase in HVAC on the fuel consumption for BEVs with their own study of five BEVs: 2018 BMW i3, 2018 Chevrolet Bolt, 2018 Nissan Leaf, 2017 Tesla Model S 75D, 2017 Volkswagen (VW) e-Golf. Two of the five vehicles had heat pumps in addition to auxiliary resistive heating as heat pumps are ineffective at extremely low temperatures. The study found an increase in combined city/highway fuel consumption of 13-22% at an ambient temperature of 95°F with the air conditioning activated and a 38-77% increase at an ambient temperature of 20°F with the heating activated when compared to operation at 75°F without any HVAC active. The AAA study also found that aggressive driving increased fuel consumption for BEVs by 41-60% at 75°F, 5-27% at 20°F, and 28-60% at 95°F. Combining the two effects together, the combined city/highway fuel consumption can be increased by as much as 41-60% at 75°F, 68-103% at temperatures near 20°F, and 53-95% near 95°F. It is clear from these numbers that the current practice of dividing city and highway drive cycle test fuel consumption values by 0.7 to account for temperature and aggressive driving effects averages out a substantial dependency on ambient temperature.

A significant correction to fuel consumption is required for BEVs and PHEVs in charge-depleting mode depending on driving aggressiveness and the local weather conditions. Therefore, we will use the EPA-unadjusted fuel consumption values and modify them based on the AAA data. The combined effect is nonlinear, as an aggressive driving fuel consumption value scales differently with temperature than a combined city/highway fuel consumption value. We will apply a temperature correction in the range of 40-75% at 20°F and below, and 15-25% at temperatures of 95°F and above, with an assumed linear variation between the nominal range of 60-75°F and the hot and cold ranges. Aggressive driving will be included with a temperature-dependent enhancement of 15% at 20°F and below, 50% in the nominal temperature range of 60-75°F, and 40% at 95°F and above, with linear variation between the ranges. This methodology produces fuel consumption correction ranges that are consistent with the AAA data as shown in Tables 4 and 5. To evaluate these fuel consumption correction values, it is necessary to provide information about the local ambient temperatures where the BEV or PHEV will be operated.

TABLE 4 Combined city/highway fuel consumption correction factors.

Vehicle	20°F AAA	20°F low/high	95°F AAA	95°F low/high
2018 BMW i3	1.77	1.4/1.75	1.22	1.15/1.25
2018 Chevrolet Bolt	1.73	1.4/1.75	1.20	1.15/1.25
2018 Nissan Leaf	1.38	1.4/1.75	1.13	1.15/1.25
2017 Tesla Model S 75D	1.60	1.4/1.75	1.19	1.15/1.25
2017 VW e-Golf	1.52	1.4/1.75	1.20	1.15/1.25

Fuel economy values for an FHEV, or PHEV in charge-sustaining mode, directly use the five-cycle test data results [48] from the EPA, applying the same linear variation with temperature as is used for the BEV or PHEV in charge-depleting mode. The aggressive driving test (US06) is not run at high and low temperatures in the EPA test plan. Therefore, we will use the same ratios of temperature-dependent aggressiveness fuel consumption enhancements at 20°F and below, and 95°F and above, to the nominal temperature range enhancement, as are used for the BEV.

Local Ambient Temperatures

U.S. weather data is available from the National Oceanic and Atmospheric Administration website [49]. These data include 30-year-averaged daily minimum, maximum, and average temperature values at a large number of weather stations. The values from weather stations within an individual county are combined to produce county averages, and the county averages are combined to produce state averages. For counties without any weather stations that have the 30-year data, the corresponding state value is utilized.

Based on the time of day that the vehicle is anticipated to be operated, weights are assigned to the minimum, maximum, and average daily temperature values to calculate the total correction to the fuel consumption value based on ambient temperature.

Electricity Generation and Combustion Emissions

The BEV or PHEV in charge-depleting mode is charged via the regional electric grid of the vehicle. Calculating the associated emissions is a complex task that is often simplified by using the total electricity mix emission rate. As previously discussed in this work, this often substantially underestimates the correct emission rate for the addition of any load on the grid as electricity is not distributed with fixed ratios of the different sources, and not all sources are capable of responding to demand increases. With the daily average marginal emission rate values presented in the previous section, we can more accurately assign the appropriate emission rate for BEV or PHEV charging.

In addition to the electricity generation emissions, there are upstream emissions associated with the extraction, production, and transportation of the fuel sources used in the emitting power generation plants. Dones et al. [50] reported that upstream CO_2eq emission contributions to the total power plant emissions are 8-12.5% for coal, 12% for oil, and 17% for natural gas electricity generation. In this work, values of 10% will be used for coal and oil electricity generation and 15% for natural gas. These values are weighted by the fractions of coal, oil, and natural gas in the marginal electricity mix used for each BA group.

Due to transmission and distribution (T&D) losses in the electric grid, the electricity generation emissions must also be scaled by a factor to account for these losses. The U.S. EIA website [51] provides T&D loss data on a state-by-state basis, and the values range from 2% to 13% with the majority of the states reporting losses of around 5%.

For FHEVs, PHEVs in charge-sustaining mode, and ICEVs, the emissions from the combustion process are assumed to be 8.887 kg CO_2eq/gal for conventional gasoline. Cooney et al. [6] reported that the upstream well-to-tank CO_2 emissions in the United States for gasoline are 23.4 g CO_2eq/MJ (lower heating value), which leads to additional emissions of 2.833 kg CO_2eq/gal. For consistency with the electricity generation upstream emissions treatment, we incorporate a 24% upstream emission contribution for the vehicles utilizing ICEs along with the assumed combustion emissions.

Vehicle Production Emissions

This work will mainly focus on comparisons of the same vehicle in FHEV and BEV models, and we will present differences in the associated emissions rather than absolute values. Therefore, we will assume that the vehicle production emissions are, for the most part, very similar and can be neglected in the difference between the vehicles. A more detailed analysis of the production contribution to the total emission rate is

TABLE 5 Aggressive driving fuel consumption correction factors.

Vehicle	75°F AAA	75°F low/high	20°F AAA	20°F low/high	95°F AAA	95°F low/high
2018 BMW i3	1.55	1.5/1.5	1.95	1.61/2.01	1.95	1.61/1.75
2018 Chevrolet Bolt	1.60	1.5/1.5	2.03	1.61/2.01	1.75	1.61/1.75
2018 Nissan Leaf	1.57	1.5/1.5	1.75	1.61/2.01	1.65	1.61/1.75
2017 Tesla Model S 75D	1.41	1.5/1.5	1.68	1.61/2.01	1.53	1.61/1.75
2017 VW e-Golf	1.53	1.5/1.5	1.73	1.61/2.01	1.64	1.61/1.75

possible using the GREET2 Vehicle Cycle Model from Argonne National Laboratory [52] considering the specifics of the material composition for each vehicle as was done by Onat et al. [18], although the authors assumed that production emissions from FHEV and PHEV versions of the same vehicle were identical. The curb weight differences between the FHEV and BEV versions of the vehicles that are considered in this work after the battery pack weights are removed are less than 5%. Therefore, the production emissions should be relatively similar.

The battery production emissions will be accounted for separately between the vehicles that are compared. BEV models typically incorporate relatively large capacity battery packs, and the associated emissions for the production of these packs are substantial. Emilsson and Dahllof [5] reported that the emissions for battery pack production span in the range of 61-106 kg CO_2eq/kWh battery capacity with the low value coming from an assumption of the utilization of zero-emission electricity for battery production (0 kg CO_2eq/MWh) and the upper value from a fossil-fuel electricity source (1000 kg CO_2eq/MWh). It should be noted that an earlier report by Romare and Dahllof [53] reports a substantially higher range of 150-200 kg CO_2eq/kWh battery capacity. Emilsson and Dahllof [5] attributed this recent reduction to improvements in production processes and the exclusion of a battery-recycling emissions contribution. Kawamoto et al. [54] reported an average value for battery production emissions of 177 kg CO_2eq/kWh battery capacity based on some earlier studies. It is worth mentioning that the local marginal emission rate where the batteries are produced should be used to determine the associated battery pack production emissions, not the local average emission rate, although care should be taken to consider if the marginal emission rate should be treated as a constant value, considering the size of the load that a battery production facility may place on the local electricity grid.

The uncertainty in the battery pack production emissions is relatively high. Nonetheless, we will use the Emilsson and Dahllof [5] range for BEV battery pack CO_2 equivalent emissions in this work as it is more recent and provides a simple way to account for the global variation in battery pack production emissions across regions with different carbon intensities in their local electricity grid. For the FHEV and PHEV models, substantially smaller battery packs are used, and we will apply the same range of values for the battery production emissions on a per kilowatt-hour capacity basis. To combine the battery pack production emissions with the fuel consumption emissions, a battery pack life must be assumed. The packs studied here will be assumed to have a life between 105% and 160% of the vehicle manufacturer's warranty for that component. Large discrepancies between the operated battery life and the assumed battery life will lead to changes in the emission rate predictions for the BEVs due to their relatively large battery pack capacities and the associated production emissions. These discrepancies are not necessarily for reasons that are unique to the BEV. Removal of a vehicle from the fleet due to an accident or premature reduction of structural integrity from operating conditions is no more or less likely to occur for a BEV than for an FHEV, but the battery pack production CO_2 is the same whether the vehicle reaches the assumed life or not, and if it is not amortized over the assumed battery life, then the emission rate for the vehicle may be substantially higher. Similarly, a battery pack that lasts longer than 160% of the warranty period will lead to a reduction in the BEV emission rate. However, a pack that lasts 200% of the warranty period only reduces the associated contribution from battery pack production to the total emissions by 20% in comparison to a pack that lasts 160% of the warranty period (normalizing battery pack production CO_2 by 5 of 4 of the original battery life produces a contribution to the total vehicle emission rate that is 4 of 5 of the original value), and at that point, the contribution to the emission rate from battery pack production is already relatively small. There is much uncertainty in the appropriate battery pack life to use currently, but as more data becomes available on the longevity of BEV battery packs and the vehicles themselves, more appropriate values for the battery life and the contribution of the battery pack production emissions will undoubtedly emerge.

Case Studies

2020 Kia Niro

The 2020 Kia Niro is available as an FHEV with a 1.56 kWh battery pack and a BEV with a 67.5 kWh (64 kWh useable) battery pack. The combined city/highway unadjusted fuel consumption for the BEV is 21.01 kWh/100 miles and the combined city/highway unadjusted fuel economy for the FHEV is 67.29 mpg. The five-cycle fuel economy test data (FTP, HWFET, US06, SC03, Cold FTP) values are 68.2, 66.2, 45.8, 52.9, and 48.6 mpg for the FHEV. The curb weights are 3106 lb (1409 kg) and 3889 lb (1764 kg) for the FHEV and BEV, respectively, and, after removing the battery pack weights, 3033 lb (1376 kg) and 2881 lb (1307 kg), respectively. The base manufacturer's suggested retail price (MSRP) values are $24,590 and $39,090 for the FHEV and BEV, respectively.

The temperature-dependent fuel consumption correction values for both driving aggressiveness and ambient temperature for both vehicle types are calculated based on the average, minimum, and maximum temperature values for each day, and are then averaged over the entire year. The weights for the three fuel consumption correction values are then set to 0.4, 0.5, and 0.1, respectively, for both the driving aggressiveness and ambient temperature corrections, to model a vehicle that is driven mostly in the mornings and evenings as part of a normal commute. Finally, the driving aggressiveness correction is scaled by a factor of one-half to indicate that aggressive driving occurs for half of the vehicle operation time.

The battery warranty extends to 100,000 miles. Therefore, the battery life will be assumed to be in the range of 105,000-160,000 miles. The upper end of this range approximately corresponds to a vehicle of the current U.S. fleet average age

(12.1 years) [55] driven the average mileage (13,500 miles) [56] each year.

The calculation of the emission rate on a per kilometer basis for the BEV is performed using the following equation:

$$ER_{BEV} = EC(1+TC)(1+AC)\frac{EER}{(1-UE)(1-T\,\&\,D)} + \frac{BPCO_2}{BL} = CEC \cdot CEER + \frac{BPCO_2}{BL} \quad \text{Eq. (16)}$$

where EC is the unadjusted combined city/highway electricity consumption in kWh/km, TC is the ambient temperature correction as a fraction, AC is the driving aggressiveness correction as a fraction, $T\,\&\,D$ is the electricity transmission and distribution loss as a fraction, EER is the electricity emission rate in kg CO_2eq/kWh, UE is the electricity upstream emissions factor as a fraction, $BPCO_2$ is the battery pack production kg CO_2eq, and BL is the useful battery life in kilometers. Some of the contributions are combined in Equation 16 so that it can be written in terms of a corrected electricity consumption, CEC, and a corrected electricity emission rate, $CEER$. The $CEER$ values combine the marginal emission rates for the BA groups and the associated upstream emissions factor as calculated from the marginal electricity mix with the T&D losses and are shown in Figure 17(a) for the statistically significant marginal source methodology and in Figure 17(b) for the emitting marginal source methodology. The $CEER$ values vary strongly between regions, indicating that conclusions on the superior vehicle choice for reducing CO_2 emissions are region dependent. For most regions, the $CEER$ values in Figure 17(b) are only slightly higher than those in Figure 17(a). The Pacific Northwest region (BPAT BA group) shows the biggest discrepancy due to the removal of hydro and wind from the marginal source category, and the Great Plains (SWPP BA group) also shows a substantial difference without wind in the marginal. As the wind is intermittent and hydro is capacity limited, it is not unreasonable to consider the sensitivity to excluding them entirely from the marginal. However, the Pacific Northwest would be able to effectively increase its hydro capacity by reducing exports to other regions making the Figure 17(a) $CEER$ values more relevant.

The emission rate on a per kilometer basis for the FHEV is calculated as

$$ER_{FHEV} = FC(1+TC)(1+AC)\cdot\frac{GER}{1-UE} + \frac{BPCO_2}{BL} = CFC \cdot CGER + \frac{BPCO_2}{BL} \quad \text{Eq. (17)}$$

where FC is the unadjusted FHEV combined city/highway fuel consumption in gallons per kilometer (gal/km), GER is the gasoline CO_2eq emission rate equal to 8.887 kg CO_2eq/gal, and UE is the upstream emissions factor as a fraction equal to 0.24. For consistency with Equation 16, terms in Equation 17 are combined into a corrected fuel consumption CFC and a corrected gasoline emission rate $CGER$ equal to 11.72 kg CO_2eq/gal.

Because of the assumed ranges for some of the terms in Equations 16 and 17, low and high ER_{BEV} values are produced along with low and high ER_{FHEV} values. The low values correspond to the most favorable set of assumptions for minimizing the GHG emissions from the individual vehicles, i.e., lowest battery pack production emissions and electricity/fuel consumption corrections, while the high values are least favorable. Due to the use of the five-cycle test data for the FHEV CFC calculation, the difference between low and high ER_{FHEV} values is exclusively due to the battery pack production contribution, which has a much smaller range than the corresponding range for the BEV. The battery pack production contribution to the emission rate for the Niro BEV ranges from 16.0 g to 42.1 g CO_2eq/km, while the FHEV range is only 0.37 g to 0.98 g CO_2eq/km. To compare the emission rates for the BEV and FHEV versions of the same vehicle, the difference between the values is reported in this work as $ER_{FHEV} - ER_{BEV}$. As a result of the much smaller difference between low and high ER_{FHEV} values, these comparisons are effectively comparisons under most BEV-favorable and least BEV-favorable assumptions.

Figure 18(a) shows the difference between the FHEV and BEV emission rates on a per kilometer basis for the Kia Niro using the most BEV-favorable values for the various ranges in Equations 16 and 17 and the statistically significant source

FIGURE 17 U.S. CEER (kg CO_2eq/MWh) (a) statistically significant source marginal, (b) emitting source marginal.

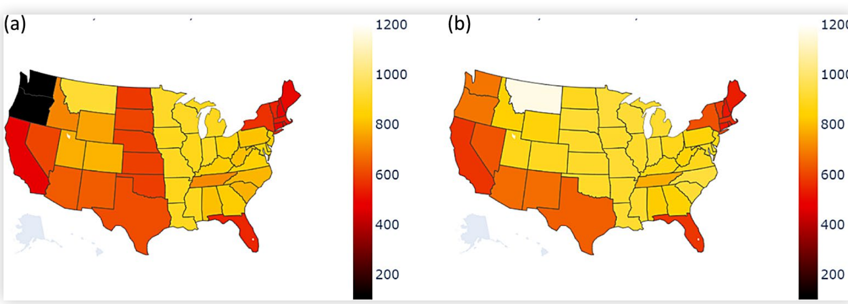

FIGURE 18 2020 Kia Niro $ER_{FHEV} - ER_{BEV}$ emission rate difference (g CO_2eq/km). (a) most BEV-favorable, statistically significant source marginal; (b) least BEV-favorable, statistically significant source marginal; (c) most BEV-favorable, emitting source marginal; (d) least BEV-favorable, emitting source marginal.

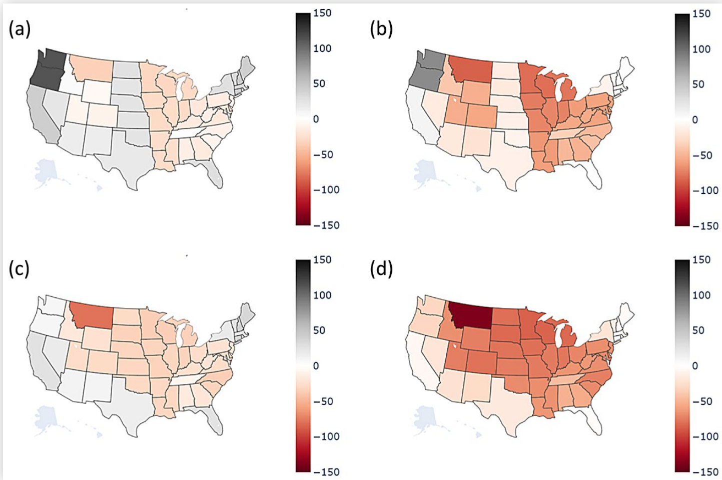

marginal emission rate. Note that positive values indicate that the BEV produces less CO_2 and are shown in shades of gray. Negative values indicate that the FHEV produces less CO_2 and are shown in shades of red. Washington state produces the best result for the BEV at +112 g CO_2eq/km while Montana produces the best result for the FHEV at −35 g CO_2eq/km. Figure 18(b) shows a similar plot with the least BEV-favorable values from the assumed ranges. Oregon produces the best result for the BEV at +85 g CO_2eq/km while Montana produces the best result for the FHEV at −87 g CO_2eq/km. The statistically significant source marginal maps reveal that the FHEV is favorable under all the considered conditions in 26 states while the same is true for the BEV in eight states. When compared based on the total demand data in Table 2, the FHEV is favorable under all conditions for regions accounting for 2107 TWh of demand while the BEV is favorable under all conditions for 790 TWh of demand. The same two plots are shown for the emitting source marginal emission rate in Figure 18(c) and (d). Under the most BEV-favorable conditions, the best result for the BEV is New Hampshire at +38 g CO_2eq/km while Montana produces the best result for the FHEV at −76 g CO_2eq/km. Under the least BEV-favorable conditions, the best result for the BEV is Connecticut at −1 g CO_2eq/km while Montana produces the best result for the FHEV at −138 g CO_2eq/km. With the emitting source marginal emission rate, the FHEV is favorable under all the considered conditions in 33 states (2660 TWh of demand) while the BEV is not favorable under all conditions in any states.

As a consistency check on the *TC* and *AC* models, we calculate simple averages of the CEC and corrected fuel economy (from corrected fuel consumption) values across all states and both high and low values in Tables 4 and 5 (for the BEV). The average *CEC* value for the Niro BEV is 30.2 kWh/100 miles, which compares well with the EPA-adjusted electricity consumption value of 30.0 kWh/100 miles. Similarly, the average corrected fuel economy for the Niro FHEV is 50.1 mpg, which compares well with the EPA-adjusted fuel economy value of 50.4 mpg. The lowest *CEC* values for the BEV occur in Florida with a range of 26.9-27.6 kWh/100 miles while the highest *CEC* values occur in Wyoming with a range of 29.6-34.2 kWh/100 miles. The highest corrected fuel economy for the FHEV occurs in Florida at 52.8 mpg while the lowest value occurs in Wyoming at 48.5 mpg.

2020 Hyundai Ioniq

The 2020 Hyundai Ioniq is available as an FHEV with a 1.56 kWh battery pack and a BEV with a 40.4 kWh (38.3 kWh useable) battery pack. The combined city/highway unadjusted fuel consumption for the BEV is 17.77 kWh/100 miles and the combined city/highway unadjusted fuel economy is 77.19 mpg for the FHEV. The five-cycle fuel economy test data (FTP, HWFET, US06, SC03, Cold FTP) values are 75.7, 79.1, 52.9, 58.9, and 52.7 mpg for the FHEV. The curb weights are 2996 lb (1359 kg) and 3371 lb (1529 kg) for the FHEV and BEV, respectively. The base price MSRP values are \$23,200 and \$33,045 for the FHEV and BEV, respectively.

The assumptions for the BEV fuel consumption corrections for the Ioniq are the same as those for the Niro, and the battery life is also assumed to span the same range as the Niro. The battery pack production contribution to the emission rate for the Ioniq BEV ranges from 9.6 g CO_2eq/km to 25.2 g CO_2eq/km, while the FHEV range is 0.37 g CO_2eq/km to 0.98 g CO_2eq/km.

Figure 19(a) shows the difference between the FHEV and BEV emission rates on a per kilometer basis for the Hyundai Ioniq using the most BEV-favorable values for the various ranges in Equations 16 and 17 and the statistically significant source marginal emission rate. Oregon produces the best result for the BEV at +104 g CO_2eq/km while Montana

FIGURE 19 2020 Hyundai Ioniq $ER_{FHEV} - ER_{BEV}$ emission rate difference (g CO_2eq/km). (a) Most BEV-favorable, statistically significant source marginal; (b) least BEV-favorable, statistically significant source marginal; (c) most BEV-favorable, emitting source marginal; (d) least BEV-favorable, emitting source marginal.

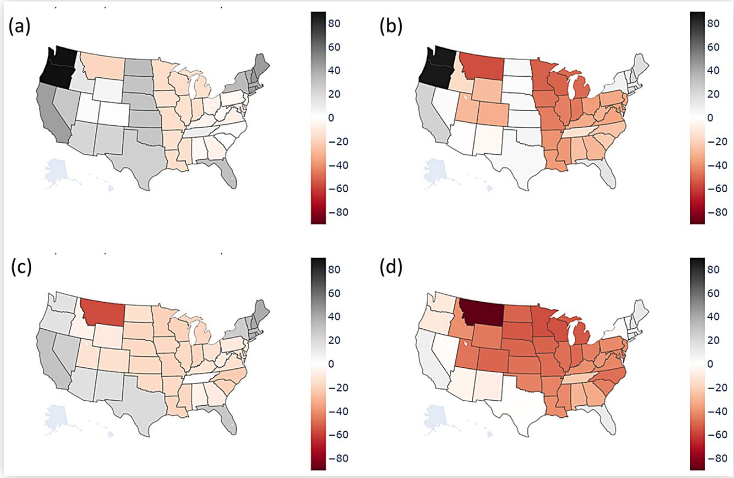

produces the best result for the FHEV at −19 g CO_2eq/km. Figure 19(b) shows a similar plot with the least BEV-favorable values from the assumed ranges. Oregon produces the best result for the BEV at +87 g CO_2eq/km while Montana produces the best result for the FHEV at −56 g CO_2eq/km. The statistically significant source marginal maps show that the BEV is favorable under all the considered conditions in 18 states (1735 TWh of demand), while the FHEV achieves the same in 22 states (1765 TWh of demand). The same two plots are shown for the emitting source marginal emission rate in Figure 19(c) and (d). Under the most BEV-favorable conditions, the best result for the BEV is New Hampshire at +42 g CO_2eq/km while Montana produces the best result for the FHEV at −57 g CO_2eq/km. Under the least BEV-favorable conditions, the best result for the BEV is Connecticut at +15 g CO_2eq/km while Montana produces the best result for the FHEV at −100 g CO_2eq/km. With the emitting source marginal emission rate, the FHEV is favorable under all the considered conditions in 32 states (2396 TWh of demand) while the BEV is favorable under all conditions in 8 states (783 TWh of demand).

Identical consistency checks were applied to the *TC* and *AC* models for the Ioniq vehicles as were done previously for the Niro vehicles. The average *CEC* value for the Ioniq BEV is 25.5 kWh/100 miles, which compares well with the EPA-adjusted electricity consumption value of 25.4 kWh/100 miles. Similarly, the average corrected fuel economy value for the Ioniq FHEV is 57.0 mpg, which compares well with the EPA-adjusted fuel economy value of 57.8 mpg. The lowest *CEC* values for the BEV occur in Florida with a range of 22.7−23.4 kWh/100 miles while the highest *CEC* values occur in Wyoming with a range of 25.0−28.9 kWh/100 miles. The highest corrected fuel economy for the FHEV occurs in Florida at 61.0 mpg while the lowest value occurs in Wyoming at 54.7 mpg.

Grid Decarbonization

The maps in Figures 18 and 19 reveal that there are regions where a consumer would most likely achieve a CO_2 emission rate reduction from the use of a BEV model instead of an FHEV model for the vehicles studied here, depending on the marginal source selection methodology, even though we have not considered the effect of future grid decarbonization. However, extending that conclusion to all electric vehicles in all U.S. regions is not supported by the data. Indeed, many regions show higher CO_2 emission rates for the BEVs in this study.

Moving into the future, large-scale adoption of BEVs and other electrification efforts will move the total demand ranges above those in the 2019 data, but we do not know what the net result of increased grid utilization from BEVs combined with the closure of some coal plants, the addition of natural gas plants, and increased renewable electricity will mean for the marginal demand and the associated emissions. Without multiple years of marginal emission rate data to determine trends, forecasts are just guesses. The standard forecasting approach [8, 57] is to use a declining average mix emission rate based on assumed future generation fractions of the emitting and non-emitting electricity sources. However, given the large errors reported here between the average mix emission rate and the marginal emission rate for present-day U.S. grids, and the inability of the average mix assumptions to capture the correct emission rate modifications associated with additional renewable generation capacity, the value of such studies is minimal. In general, solutions to an initial value problem with initial conditions that are low by 16-67% (see Table 2) and incorrect modeling of the associated source terms are not expected to produce meaningful results.

The results from the case studies presented so far set an appropriate initial value for vehicle comparisons and answer the question "Using recent grid data emission rates which have a relatively high degree of certainty, how do BEV and FHEV models compare to one another on an emissions basis?". However, these results may only be accurate for a short duration of the grid changes substantially, and we can calculate the required reduction in the vehicle lifetime average marginal emission rate for the BEV to achieve total emissions parity with the FHEV. For this purpose, we consider a vehicle lifetime of 18 years and 210,000 miles. Due to this duration, both vehicles require a single battery replacement, at 105,000 miles for the least BEV-favorable assumptions and 160,000 miles for the most-BEV favorable assumptions. These batteries will most likely be sourced more efficiently and produced using electricity from a decarbonized grid and are, therefore, expected to have a reduced emissions footprint. The most BEV-favorable battery production value for the battery replacement is reduced by 10% to account for the improvements in material sourcing (the original value already assumes zero-emission electricity for the battery production). The least BEV-favorable battery production value for the replacement also includes an additional 15% reduction for the production electricity utilization based on the grid decarbonization. Therefore, the battery replacement production emissions range is adjusted to 55-93 kg CO_2eq/kWh battery capacity.

The marginal emission rate percent reductions (from the 2019 grid calculated values) required for BEV-FHEV total emissions parity are shown in Figure 20 for the Kia Niro and in Figure 21 for the Hyundai Ioniq for both most BEV-favorable assumptions and least BEV-favorable assumptions under the statistically significant source classification. The figures present the required percent reduction in the vehicle lifetime average electricity marginal emission rate value and the corresponding final year percent reduction (from the 2019 grid calculated value) under the assumption of a constant year-over-year fractional reduction to match the required vehicle lifetime average reduction. The influence of battery pack capacity can be seen in Figures 20 and 21, i.e., the Kia Niro requires larger reductions in the marginal emission rate to achieve total emissions parity than the Hyundai Ioniq.

Figure 20(a) shows that a reduction of 24.6% in the vehicle lifetime average (45.2% final year) marginal emission rate will lead to BEV parity or superiority in all regions for the Kia Niro for the most BEV-favorable assumptions, and a reduction of 43.1% (72.6% final year) is required to achieve the same for the least BEV-favorable assumptions in Figure 20(b). Corresponding values for the Hyundai Ioniq are 16.2% (30.7% final year) and 33.3% (58.8% final year) from Figure 21(a) and (b), respectively. The International Energy Agency's Stated Policy Scenario (STEPS) leads to a projection that changes in the U.S. average electricity mix will produce a drop of approximately 20% in the vehicle lifetime average (starting in 2021) of the average mix emission rate [8]. However, given the large differences between the average mix and marginal emission rates calculated from recent grid data, it is unlikely that the reduction in the vehicle lifetime average of the marginal emission rate bears any substantial connection to this value or any other average mix calculated value.

While it is beyond the scope of the present work to project the contiguous U.S. grid marginal emission rates over a vehicle lifetime, it is important to assess if the reduction ranges from the previous paragraph are a foregone conclusion or if it is unlikely that they can be reached. Therefore, we use the 2019 MISO BA group dataset and scale the coal, natural gas, nuclear, oil, hydro, solar, and wind sources with the EIA projections for U.S. source generation in 2022 and 2023 [58]. All imports and other sources remain the same, and the demand is scaled by the projected increase in total generation. These years were selected as the projections should have the least uncertainty. The most recent data indicate that the 2021 EIA projections appear to have overpredicted coal generation by 3% and underpredicted natural gas generation by 10%. The generation-only values for the marginal emission rate for 2022

FIGURE 20 Marginal emission rate (statistically significant source classification) percent reduction required for emissions parity between BEV and FHEV models of the 2020 Kia Niro. (a) Most BEV-favorable, vehicle lifetime average; (b) least BEV-favorable, vehicle lifetime average; (c) most BEV-favorable, final year; (d) least BEV-favorable, final year.

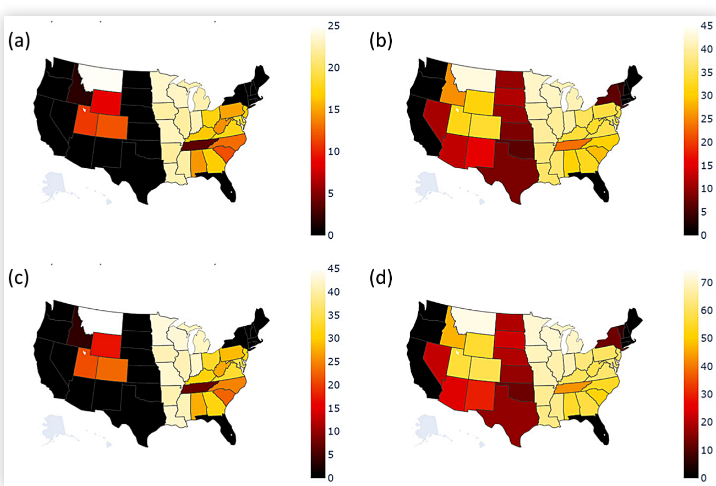

FIGURE 21 Marginal emission rate (statistically significant source marginal) percent reduction required for emissions parity between BEV and FHEV models of the 2020 Hyundai Ioniq. (a) Most BEV-favorable, vehicle lifetime average; (b) least BEV-favorable, vehicle lifetime average; (c) most BEV-favorable, final year; (d) least BEV-favorable, final year.

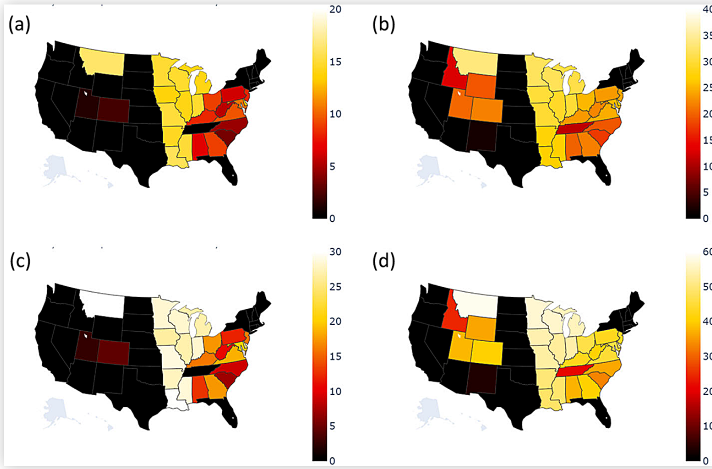

and 2023 in the MISO BA group region are 715.0 kg CO_2eq/MWh and 676.3 kg CO_2eq/MWh, respectively. These values are 4.6% and 9.8% lower than the 2019 generation-only value in Table 2. For a constant annual reduction rate, the ranges required for the BEV models to achieve emissions parity with the FHEV models are 3.2-6.8% for the Kia Niro, and 1.8-4.6% for the Hyundai Ioniq, where the range is associated with most BEV-favorable and least-BEV favorable assumptions for the comparison.

There are many limitations to the approach in the previous paragraph as scaled past data does not represent future grid data accurately and the forecasts for the U.S. grid are not necessarily relevant for any individual regional grid. The 2023 wind generation fraction in the scaled data is 14%, but the wind is not acting as a marginal source. Without real grid data, it will not be possible to incorporate the demand response of the wind source into the analysis if it occurs. We can say with confidence that the Hyundai Ioniq BEV has a much better chance than the Kia Niro BEV of achieving emissions parity with the hybrid equivalents over the vehicle lifetime. However, after accounting for the associated uncertainties in the projections, it is not clear that the BEV models of these particular vehicles will reach emissions parity in the MISO BA group region. The estimated average mix emission rates from the scaled datasets are 552 kg CO_2eq/MWh and 516 kg CO_2eq/MWh for 2022 and 2023, respectively. The use of these emission rates would incorrectly lead to a high degree of confidence in the conclusion that all BEVs are guaranteed to achieve reduced emissions over the vehicle lifetime in comparison to HEVs.

Due to the uncertainty in many regions of the United States on when the local grid will be able to provide an emissions reduction for a BEV in comparison to an FHEV, the benefits of PHEVs become evident. Many PHEVs provide 30-50 miles of charge-depleting operation with a battery pack that is often less than half the size of a similar BEV model. PHEVs suffer from reduced charge-sustaining operation fuel economy due to increased weight over an FHEV and incur larger battery pack production emissions than the FHEV. However, the ability to switch to mostly charge-depleting operation over typical commute distances when the grid is ready, especially in the regions that are currently far from achieving BEV-FHEV total emissions parity, may allow them to operate with lower total emissions than either the BEV or the FHEV over their lifetime.

Here we compare the 2021 VW ID.4 BEV (82.4 kWh pack) with the Toyota RAV4 Prime PHEV (18.1 kWh pack) which are all-wheel-drive vehicles with very similar physical dimensions. We use the same assumptions in the comparison as were applied in the Kia Niro and Hyundai Ioniq case studies, but the results are presented in terms of the fuel economy that the PHEV would need to achieve to match the GHG emissions of the BEV in Figure 22. Figure 22(a) and (b) use marginal emission rates, while Figure 22(c) and (d) and use average mix emission rates. The EPA combined fuel economy rating for the PHEV is 38 mpg, indicating that there are large parts of the U.S. grid where the RAV4 PHEV is currently superior on an emissions basis to the VW ID.4 when the more accurate marginal emission rates are applied. The average mix emission rates lead to the conclusion that the PHEV is barely competitive over a much smaller area, which highlights the BEV-favorable bias of these less accurate emission rates.

The vehicle studies presented in this work make evident that the BEV versus HEV debate in most of the United States should remain an open topic of research if minimizing total CO_2 emissions is indeed the goal. All or nothing approaches may provide simplicity in policy making, but the associated technological development suppression penalty associated with a narrow focus could prove to be substantial. Even in areas where the BEV is currently superior on a GHG emissions basis, carbon-free and carbon-neutral fuels and improved engine efficiency [1] may eventually allow HEVs to become

FIGURE 22 All-wheel-drive Toyota RAV4 Prime PHEV equivalent GHG emission fuel economy (mpg) when compared to VW ID.4 BEV. (a) Most BEV-favorable, statistically significant marginal emission rates; (b) least BEV-favorable, statistically significant marginal emission rates; (c) most BEV-favorable, average mix emission rates; (d) least BEV-favorable, average mix emission rates.

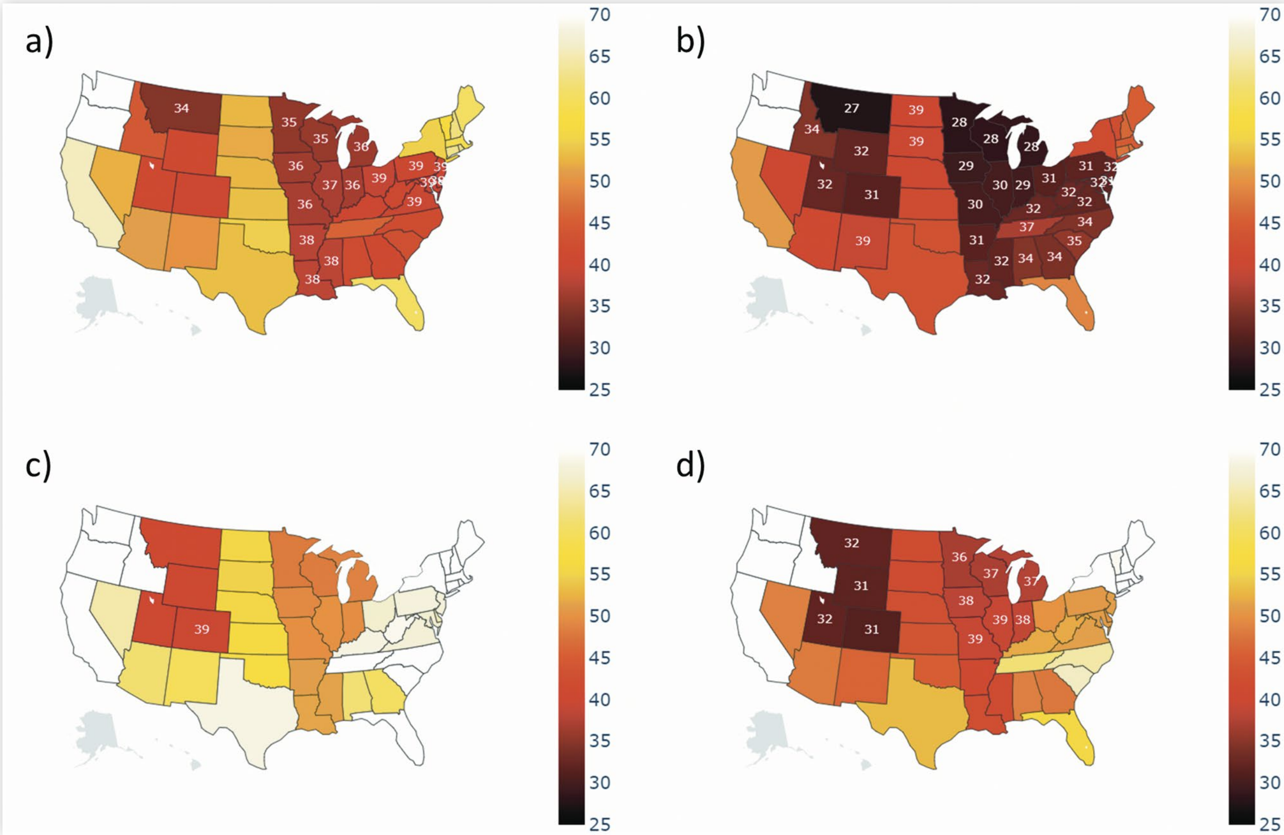

competitive, just as grid decarbonization may lead to a broader geographic area over which the BEV is a better option. The accuracy of vehicle comparison efforts will improve and provide greater certainty in the conclusions than can be achieved today. The use of the methodology presented in this work to track the changing U.S. grid marginal emission rate is a vital part of the move toward a more accurate vehicle LCA.

Conclusions

Keeping in mind the quote "All models are wrong but some are useful," attributed to British statistician George E. P. Box, the main conclusions of this work are as follows:

1. A vehicle equivalent CO_2 emissions comparison between a BEV and an FHEV is an environmental opportunity cost calculation that requires the determination of the marginal emission rate for the electricity supplying the BEV to be compared to the known emission rate for the combustion process in an HEV.
2. U.S. vehicle comparisons using the average mix emission rate introduce large errors. Projections based on assumed future average electricity mix compositions are not expected to achieve predictive results.
3. Ongoing grid decarbonization efforts will require that the marginal emission rates be recalculated each year to reassess the environmental impact of BEVs. Safe harbor statements that increased renewable generation in the future will, by default, justify the required infrastructure changes, and the transformation of the fleet to predominantly EVs are a drastic oversimplification that requires validation from available data and should be treated with an appropriate level of skepticism until reliable regional trends in the U.S. grid decarbonization effort can be established.
4. The practical methodology applied in this work to compare vehicle equivalent CO_2 emissions includes the lower-order terms which have the biggest impact on the final result. It is not meant to replace full vehicle LCAs but rather provides an accounting of vehicle GHG emissions that can be easily understood by consumers. More detailed studies are vital to guide decision-making when higher-order terms must be considered, or for providing information for the lower-order terms. Many other dimensions can

be considered, besides equivalent CO_2 emissions, with more detailed LCAs.

5. For the case studies considered here, the selection of an FHEV is more likely to achieve a GHG emissions benefit in comparison to a BEV when using present-day marginal emission rates, but there are substantial regional and vehicle model dependencies. When using the statistically significant marginal source classification, regions accounting for approximately 44% of the total 2019 U.S. electricity demand would be best served on an equivalent CO_2 emissions basis by an Ioniq FHEV under all reasonable ranges of assumptions (battery life, battery production CO_2, corrected electricity and fuel consumption values), while the same is true for the Ioniq BEV in regions accounting for 43% of the electricity demand. For the remaining portion of the electricity demand, the superior vehicle technology depends on the assumptions. If the more restrictive emitting source marginal classification is used, then the advantageous demand percentages for the FHEV and the BEV change to 60% and 19%, respectively. While there are regions where an Ioniq BEV may be favorable to the FHEV, current automotive industry trends are moving toward vehicles with larger battery packs. For the Niro with a larger battery pack, the use of the statistically significant marginal source classification indicates that approximately 52% of the total 2019 U.S. electricity demand would be best served on an equivalent CO_2 basis by a Niro FHEV under all reasonable ranges of assumptions, while the same is true for the Niro BEV in regions accounting for 20% of the electricity demand. If the emitting source marginal classification is used, then the advantageous demand percentages for the FHEV and the BEV change to 66% and 0%, respectively.
6. Regional grid marginal emission rate reductions of 30.7-58.8% (from the 2019 values) by the final year of an assumed 18-year vehicle lifetime will lead the Ioniq BEV to achieve emissions superiority over the FHEV in all regions. The corresponding reduction range for the Niro BEV is 45.2-72.6%. Projections for grid decarbonization are currently based on the average mix emission rate and are, therefore, not relevant for the marginal emission rate. Due to the uncertainty in the ability of the most carbon-intensive regional grids to achieve these emission rate reductions, a PHEV may be an appropriate hedge that provides the flexibility to take advantage of the switch from FHEV-superior to BEV-superior operation windows in the middle of the vehicle lifetime.

In summary, there is limited evidence that immediate widespread adoption of BEVs in the United States will lead to a substantial positive impact on GHG emissions over vehicle lifetimes in the near term in comparison to FHEV and PHEV alternatives, especially after considering the emissions cost of the required infrastructure upgrades. This is not meant to imply that there is no role for BEVs to play, but rather that the scope of application requires substantial modification to be consistent with the realities of the current electricity supply infrastructure and operation. It goes without saying that the decision to drive less is far more beneficial for the environment than the decision to purchase a particular vehicle powertrain.

Acknowledgments

The authors wish to thank Dr. Paul Miles of Sandia National Laboratories for providing feedback on the manuscript and Atley Atienza of Greenhills School for assistance with the data processing.

References

1. Senecal, K. and Leach, F., *Racing toward Zero: The Untold Story of Driving Green* (Warrendale, PA: SAE International, 2021), ISBN:978-1-4686-0146-6.
2. Senecal, P.K. and Leach, F., "Diversity in Transportation: Why a Mix of Propulsion Technologies Is the Way forward for the Future Fleet," *Results in Engineering* 4 (2019): 100060, https://doi.org/10.1016/j.rineng.2019.100060.
3. Leach, F., Kalghati, G., Stone, R., and Miles, P., "The Scope for Improving the Efficiency and Environmental Impact of Internal Combustion Engines," *Transportation Engineering* 1 (2020): 100005, https://doi.org/10.1016/j.treng.2020.100005.
4. Yuksel, T., Tamayao, M.-A.M., Hendrickson, C., Azevedo, I.M.I. et al., "Effect of Regional Grid Mix, Driving Patterns and Climate on the Comparative Carbon Footprint of Gasoline and Plug-In Electric Vehicles in the United States," *Environmental Research Letters* 11, no. 4 (2016): 044007, https://doi.org/10.1088/1748-9326/11/4/044007.
5. Emilsson, E. and Dahllof, L., *Lithium-Ion Vehicle Battery Production* (Stockholm: IVL Swedish Environmental Research Institute, 2019)
6. Cooney, G., Jameison, M., Marriott, J., Bergerson, J. et al., "Updating the U.S. Life Cycle GHG Petroleum Baseline to 2014 with Projections to 2040 Using Open-Source Engineering-Based Models," *Environmental Science & Technology* 51 (2017): 977-987, https://doi.org/10.1021/acs.est.6b02819.
7. Marmiroli, B., Messagie, M., Dotelli, G., and Van Mierlo, J., "Electricity Generation in LCA of Electric Vehicles: A Review," *Applied Sciences* 8 (2018): 1384, https://doi.org/10.3390/app8081384.
8. Bieker, G., "A Global Comparison of the Life-Cycle Greenhouse Gas Emissions of Combustion Engine and Electric Passenger Cars," July 2021, accessed November 1, 2021, http://theicct.org/sites/default/files/publications/Global-LCA-passenger-cars-jul2021_0.pdf.
9. Muratori, M., Alexander, M., Arent, D., Bazilian, M. et al., "The Rise of Electric Vehicles—2020 Status and Future Expectations," *Progress in Energy* 3, no. 2 (2021): 022002.
10. U.S. Energy Information Administration, "Electricity Explained, Electricity in the United States," March 20, 2020,

accessed October 5, 2020, http://www.eia.gov/energyexplained/electricity/electricity-in-the-us.php.

11. U.S. Energy Information Administration, "How Much Carbon Dioxide Is Produced per Kilowatthour of U.S. Electricity Generation," February 20, 2020, accessed October 6, 2020, http://www.eia.gov/tools/faqs.
12. U.S. Environmental Protection Agency, "eGRID2018 Summary Tables," accessed October 1, 2020, http://www.epa.gov/sites/production/files/2020-01/documents/egrid2018_summary_tables.pdf.
13. Noori, M., Gardner, S., and Tatari, O., "Electric Vehicle Cost, Emissions, and Water Footprint in the United States: Development of a Regional Optimization Model," *Energy* 89 (2015): 610-625, https://doi.org/10.1016/j.energy.2015.05.152.
14. Mayyas, A., Omar, M., Hayajneh, M., and Mayyas, A., "Vehicle's Lightweight Design vs. Electrification from Life Cycle Assessment Perspective," *Journal of Cleaner Production* 167 (2017): 687-701, https://doi.org/10.1016/j.jclepro.2017.08.145.
15. Corradi, O., "Marginal Emissions: What They Are, and When to Use Them," June 13, 2019, accessed October 15, 2020, http://electricitymap.org/blog/marginal-emissions-what-they-are-and-when-to-use-them/.
16. U.S. Energy Information Administration, "Annual Energy Outlook 2007 with Projections to 2030," U.S. Department of Energy, Washington, DC, 2007.
17. Ma, H., Balthasar, F., Tait, N., Riera-Palou, X. et al., "A New Comparison between the Life Cycle Greenhouse Gas Emissions of Battery Electric Vehicles and Internal Combustion Vehicles," *Energy Policy* 44 (2012): 160-173, https://doi.org/10.1016/j.enpol.2012.01.034.
18. Onat, N., Kuckukvar, M., and Tatari, O., "Conventional, Hybrid, Plug-In Hybrid or Electric Vehicles? State-Based Comparative Carbon and Energy Footprint Analysis in the United States," *Applied Energy* 150 (2015): 36-49, https://doi.org/10.1016/j.apenergy.2015.04.001.
19. Samaras, C. and Meisterling, K., "Life Cycle Assessment of Greenhouse Gas Emissions from Plug-In Hybrid Vehicles: Implications for Policy," *Environmental Science Technology* 42, no. 9 (2008): 3170-3176, https://doi.org/10.1021/es702178s.
20. Hadley, S. and Tsvetkova, A., "Potential Impacts of Plug-In Hybrid Electric Vehicles on Regional Power Generation," *The Electricity Journal* 22, no. 10 (2008): 56-68, https://doi.org/10.1016/j.tej.2009.10.011.
21. Kintner-Meyer, M., Davis, S., Sridhar, S., Bhatnagar, D. et al., "Electric Vehicles at Scale—Phase I Analysis: High EV Adoption Impacts on the Western U.S. Power Grid," Pacific Northwest National Laboratory, 2020.
22. U.S. Environmental Protection Agency, "AVERT User Manual," September 2020, accessed July 2021, http://www.epa.gov/avert/avert-user-manual.
23. Broekhoff, D., "The Greenhouse Gas Protocol: Guidelines for Quantifying GHG Reduction from Grid-Connected Electricity Projects," World Resources Council and the World Business Council for Sustainable Development, 2007, accessed October 1, 2020, http://pdf.wri.org/GHGProtocol-Electricity.pdf.
24. U.S. Environmental Protection Agency, "eGrid Technical Support Document," January 2020, accessed October 1, 2020, http://www.epa.gov/egrid/egrid-technical-support-document.
25. Ryan, N.A., Johnson, J.X., and Keoleian, G.A., "Comparative Assessment of Models and Methods to Calculate Grid Electricity Emissions," *Environmental Science & Technology* 50, no. 17 (2016): 8937-8953, https://doi.org/10.1021/acs.est.5b05216.
26. U.S. Environmental Protection Agency, "Air Markets Program Data," accessed January 16, 2021, http://ampd.epa.gov/ampd/.
27. U.S. Energy Information Administration, "Form EIA-923 Detailed Data with Previous Form Data (EIA-906/920)," accessed October 1, 2020, http://www.eia.gov/electricity/data/eia923/.
28. CISO, "California ISO," accessed October 1, 2020, http://www.caiso.com/Pages/default.aspx.
29. California, "Exec. Order No. N-79-20," September 23, 2020.
30. California Energy Commission, "2018 Total System Electric Generation," June 24, 2019, accessed January 31, 2021, http://www.energy.ca.gov/data-reports/energy-almanac/california-electricity-data/2020-total-system-electric-generation/2018.
31. U.S. Energy Information Administration, "State Energy Data System (SEDS): 1960-2018: Sector End-Use: Table CT7," June 26, 2020, accessed January 31, 2021, http://www.eia.gov/state/seds/sep_use/total/pdf/use_CA.pdf.
32. Wolfram, P. and Lutsey, N., "Electric Vehicles: Literature Review of Technology Costs and Carbon Emissions," The International Council on Clean Transportation (ICCT), Washington, DC, 2016.
33. Anthanasopoulou, L., Bikas, H., and Starvopoulos, P., "Comparative Well-to-Wheel Emissions Assessment of Internal Combustion Engine and Battery Electric Vehicles," *Procedia CIRP* 78 (2018): 25-30, https://doi.org/10.1016/j.procir.2018.08.169.
34. Miller, M., Holmes, A., Colon, B., and Savagian, P., "The GM 'Voltec' 4ET50 Multi-Mode Electric Transaxle," *SAE Int. J.*

Engines 4, no. 1 (2011): 1102-1114, https://doi.org/10.4271/2011-01-0887.

35. California Energy Commission, "QFER CEC-1304 Power Plant Owner Reporting Database: Annual Generation," May 4, 2020, accessed January 31, 2021, http://ww2.energy.ca.gov/almanac/electricity_data/web_qfer/Annual_Generation_cms.php?goSort=annual.plantID&year=2018.
36. Koohi-Fayegh, S. and Rosen, M.A., "A Review of Energy Storage Types, Applications and Recent Developments," *Journal of Energy Storage* 27 (2020): 101047, https://doi.org/10.1016/j.est.2019.101047.
37. California Energy Commission, "Total System Electric Generation," 2019, accessed October 1, 2020, http://www.energy.ca.gov/data-reports/energy-almanac/california-electricity-data/2020-total-system-electric-generation/2019.
38. U.S. Energy Information Administration, "Hourly Electric Grid Monitor," accessed October 8, 2020, http://www.eia.gov/electricity/gridmonitor/dashboard/electric_overview/US48/US48.
39. U.S. Energy Information Administration, "Hourly Electric Grid Monitor," accessed August 19, 2021, http://www.eia.gov/electricity/gridmonitor/about.
40. U.S. Energy Information Administration, "Open Data," accessed October 1, 2020, http://www.eia.gov/opendata/qb.php?category=2123635.
41. Zivin, J.S.G., Kotchen, M.J., and Mansur, E.T., "Spatial and Temporal Heterogeneity of Marginal Emissions: Implications for Electric Cars and Other Electricity-Shifting Policies," *Journal of Economic Behavior & Organization* 107 (2014): 248-268, https://doi.org/10.3386/w18462.
42. Tri-City Herald, "Hermiston Power Project to Balance Wind Output," accessed March 1, 2021, http://www.tri-cityherald.com/news/business/article31789002.html.
43. Bonneville Power Administration, "Columbia Generating Station Steps up to Ease BPA Oversupply," accessed March 1, 2021, http://www.bpa.gov/news/newsroom/Pages/Columbia-Generating-Station-steps-up-to-ease-BPA-oversupply.aspx.
44. Lattanzio, R.K. and Clark, C.E., "Environmental Impacts of Battery Electric and Internal Combustion Engine Vehicles R46420," Congressional Research Service, 2020.
45. U.S. Department of Energy, "Download Fuel Economy Data," accessed October 1, 2020, http://www.fueleconomy.gov/feg/download.shtml.
46. U.S. Department of Energy, "Detailed Test Information," accessed October 1, 2020, http://www.fueleconomy.gov/feg/fe_test_schedules.shtml.
47. American Automobile Association, "AAA Electric Vehicle Range Testing," February 2019, accessed October 1, 2020, http://www.aaa.com/AAA/common/AAR/files/AAA-Electric-Vehicle-Range-Testing-Report.pdf.
48. U.S. Environmental Protection Agency, "Data on Cars Used for Testing Fuel Economy," accessed October 1, 2020, http://www.epa.gov/compliance-and-fuel-economy-data/data-cars-used-testing-fuel-economy.
49. National Oceanic and Atmospheric Administration, "Climate Normal Data," accessed October 1, 2020, http://www.ncdc.noaa.gov/data-access/land-based-station-data/land-based-datasets/climate-normals.
50. Dones, R., Heck, T., and Hirschberg, S., "Greenhouse Gas Emissions from Energy Systems: Comparison and Overview," *Encyclopedia of Energy* 3 (2004): 77-95.
51. U.S. Energy Information Administration, "State Electricity Profiles," accessed October 1, 2020, http://www.eia.gov/electricity/state/.
52. Burnham, A., Wang, M., and Wu, Y., "Development and Applications of GREET 2.7—The Transportation Vehicle-Cycle Model," 2006.
53. Romare, M. and Dahlloff, L., *The Life Cycle Energy Consumption and Greenhouse Gas Emissions from Lithium-Ion Batteries* (Stockholm: IVL Swedish Environmental Research Institute, 2017)
54. Kawamoto, R., Mochizuki, H., Moriguchi, Y., Nakano, T. et al., "Estimation of CO_2 Emissions of Internal Combustion Engine Vehicle and Battery Electric Vehicle Using LCA," *Sustainability* 11, no. 9 (2019): 2690, https://doi.org/10.3390/su11092690.
55. Beresford, C. and Miller, C., "Average Age of Vehicles on the Road Rises above 12 Years," June 21, 2021, accessed August 20, 2021, http://www.caranddriver.com/news/a33457915/average-age-vehicles-on-road-12-years/.
56. Kopestinsky, A., "How Much Do Americans Drive?," March 5, 2021, accessed August 20, 2021, http://policyadvice.net/insurance/insights/how-much-do-americans-drive/.
57. Ricardo Energy & Environment, "Determining the Environmental Impacts of Conventional and Alternatively Fuelled Vehicles through LCA," July 2020, accessed November 1, 2021, http://op.europa.eu/en/publication-detail/-/publication/1f494180-bc0e-11ea-811c-01aa75ed71a1.
58. U.S. Energy Information Administration, "Annual Energy Outlook 2021," February 3, 2021, accessed January 1, 2022, http://www.eia.gov/outlooks/aeo/.

Appendix A

TABLE A.1 BA groups.

BA group	BAs in group	Data rejection threshold (%)	Min/max sample size
AZPS	AZPS, DEAA, EPE, GRIF, GRMA, HGMA, PNM, SRP, TEPC, WALC	4	265/311
BPAT	AVRN, AVA, BPAT, CHPD, DOPD, GCPD, GRID, PACW, PGE, PSEI, SCL, TPWR	4	302/327
CISO	BANC, CISO, IID, LDWP, TIDC	2	285/332
DUK	DUK, CPLE, CPLW, SC, SCEG, SEPA, YAD	2	223/338
ERCO	ERCO	1	362/364
FPL	FPC, FMPP, FPL, GVL, HST, JEA, NSB, SC, TAL, TEC	2	285/320
IPCO	IPCO	1	360/363
ISNE	ISNE	1	363/365
MISO	AECI, EEI, MISO, SPA	2	307/356
NEVP	NEVP	2	173/354
NWMT	GWA, NWMT, WAUW, WWA	2	307/359
NYIS	NYIS	1	359/365
PACE	PACE, PSCO, WACM	1	338/349
PJM	LGEE, PJM	2	299/327
SOCO	AEC, SOCO	2	362/365
SWPP	SWPP	2	269/297
TVA	TVA	2	179/314

Appendix B

TABLE B.1 Statistically significant source selection hourly marginal emission rates/standard errors (kg CO_2eq/MWh).

Hour	AZPS	BPAT	CISO	DUK	ERCO	FPL
1	530.5/23.0	0.0/15.9	397.7/10.7	723.7/15.2	525.7/5.4	437.5/10.3
2	517.0/24.2	0.0/16.3	398.2/11.5	697.0/15.5	520.7/5.4	433.5/10.7
3	516.5/25.4	0.0/16.3	421.3/11.6	684.0/14.9	517.3/5.3	432.2/10.7
4	522.5/25.0	3.5/15.9	426.0/12.4	676.9/14.0	516.1/5.1	431.4/10.8
5	531.3/24.3	4.1/16.2	425.7/9.6	642.0/13.7	517.3/5.2	438.8/10.4
6	515.7/22.9	6.0/14.3	375.1/12.7	617.3/12.5	518.9/5.1	436.6/9.4
7	493.7/19.4	133.1/16.3	341.2/11.2	582.7/13.9	521.0/4.7	435.3/7.3
8	496.4/18.7	110.4/16.7	337.7/9.0	585.9/13.9	522.7/4.8	430.6/7.1
9	504.8/18.4	130.1/19.4	363.9/7.5	639.2/14.4	527.7/5.2	431.0/8.6
10	531.2/17.0	186.6/22.0	379.6/7.3	714.9/14.5	529.7/5.2	438.2/10.1
11	542.2/16.6	204.3/22.8	385.5/7.6	710.7/14.7	536.9/5.2	448.4/9.9
12	556.9/15.3	192.3/23.5	385.3/7.1	700.8/13.6	475.6/31.9	456.6/9.0
13	561.9/13.7	125.1/22.3	380.9/7.0	674.4/13.1	474.4/29.3	470.6/8.4
14	567.5/13.3	126.3/20.8	382.6/6.8	654.6/12.6	477.4/27.2	473.1/8.0
15	572.4/12.9	107.1/19.0	380.1/6.7	636.5/12.0	474.9/26.4	480.8/7.6
16	579.8/13.5	104.9/18.9	376.3/6.7	642.1/11.5	484.7/24.8	483.9/7.0
17	585.0/14.0	97.7/19.5	385.8/6.8	643.6/11.8	473.8/24.9	479.8/6.8
18	578.1/15.9	123.7/20.2	402.6/7.4	654.4/12.0	481.2/24.9	483.9/7.1
19	575.1/17.6	132.4/21.8	421.8/6.8	673.1/11.6	487.5/25.8	486.5/7.4
20	563.0/19.2	146.7/23.0	442.6/7.6	700.6/11.6	529.6/4.5	488.0/7.6
21	557.7/19.9	138.2/24.3	440.6/8.1	721.0/12.5	521.1/4.4	475.9/8.1
22	546.7/21.3	129.0/27.2	431.7/8.7	743.3/13.1	522.0/4.6	453.7/9.1
23	543.9/21.6	3.5/15.6	418.8/9.7	767.8/13.2	522.1/5.0	443.5/10.9
24	559.9/21.6	0.0/15.7	409.6/10.5	748.3/13.5	524.0/5.2	417.8/10.8

TABLE B.2 Statistically significant source selection hourly marginal emission rates/standard errors (kg CO_2eq/MWh).

Hour	IPCO	ISNE	MISO	NEVP	NWMT	NYIS
1	602.8/26.5	430.4/8.2	737.5/6.9	499.0/11.9	826.9/22.2	455.3/13.3
2	603.2/25.7	421.6/8.0	723.3/7.0	510.5/12.1	828.8/22.6	429.6/12.8
3	603.9/24.4	420.3/8.1	722.9/7.4	528.8/12.5	836.0/22.4	426.4/13.1
4	613.2/24.7	421.7/8.3	723.5/7.3	539.4/12.9	831.6/21.7	422.6/13.1
5	608.4/24.7	428.7/8.4	737.1/7.3	541.6/13.3	834.5/21.4	421.5/13.4
6	606.8/25.5	410.0/6.6	736.2/6.9	525.1/13.5	831.3/21.2	431.4/16.4
7	634.2/18.4	388.3/5.1	731.9/6.8	502.9/13.1	816.2/21.5	417.9/12.6
8	658.4/18.6	375.5/5.3	744.1/7.0	497.2/11.4	819.7/21.2	400.0/11.6
9	643.9/17.2	394.5/5.1	758.0/7.6	497.7/10.6	825.5/21.9	463.8/11.0
10	645.1/16.2	405.2/4.8	763.4/7.8	505.6/10.2	819.0/22.5	466.4/13.5
11	657.9/15.8	405.1/4.5	769.5/7.2	506.0/10.0	811.6/23.1	494.9/11.2
12	654.9/15.3	411.8/6.0	758.9/6.5	496.7/10.2	810.6/22.9	498.3/11.1
13	639.1/15.7	410.5/6.1	758.5/6.4	502.2/9.6	826.5/23.3	479.9/13.0
14	680.3/14.9	405.0/5.8	756.5/6.5	505.9/9.2	828.5/23.9	487.5/11.0
15	622.1/16.4	395.0/5.6	751.0/6.3	506.7/9.7	813.2/24.3	490.5/10.7
16	601.5/16.6	383.3/4.3	754.5/8.9	505.1/10.7	802.8/24.5	503.5/11.2
17	652.5/15.5	379.9/4.6	751.4/9.2	510.0/14.2	803.1/24.6	525.2/10.8
18	656.4/15.4	383.9/5.3	737.2/9.2	521.8/14.9	814.8/24.0	528.0/10.4
19	671.4/15.6	399.6/5.6	737.4/9.1	547.1/17.3	813.9/23.0	532.4/10.7
20	692.1/16.9	413.5/5.6	755.8/9.2	558.9/19.0	823.7/21.5	528.3/10.9
21	658.1/18.4	429.7/3.3	759.1/9.6	534.5/19.9	830.1/20.8	512.8/13.0
22	630.6/28.1	440.4/6.8	778.0/6.9	495.3/14.2	833.1/20.7	540.0/11.1
23	617.3/29.8	427.5/3.6	771.7/6.9	489.0/12.9	828.2/21.0	516.0/13.6
24	587.5/28.7	421.8/9.3	760.9/7.1	493.9/12.1	782.1/24.5	487.9/13.9

TABLE B.3 Statistically significant source selection hourly marginal emission rates/standard errors (kg CO_2eq/MWh).

Hour	PACE	PJM	SOCO	SWPP	TVA
1	644.7/35.4	714.9/7.8	662.9/13.3	467.6/70.7	618.4/19.7
2	641.8/34.2	703.1/8.3	650.3/13.3	475.7/70.0	601.7/19.4
3	654.2/32.2	693.1/9.1	635.6/13.1	477.9/70.0	578.8/19.1
4	671.9/32.5	685.3/9.5	633.3/13.2	482.9/69.8	560.7/17.3
5	664.2/32.9	676.9/9.5	638.0/12.9	481.7/69.7	533.0/16.2
6	653.3/33.1	658.7/8.5	604.7/11.9	526.3/67.8	506.1/15.4
7	659.1/12.7	624.9/8.3	593.7/11.9	608.9/60.3	498.7/17.0
8	675.0/12.1	629.9/7.5	594.3/13.0	731.3/7.8	519.4/17.0
9	678.4/13.1	665.2/7.4	643.3/14.5	753.5/8.1	565.8/18.3
10	706.1/11.5	704.9/7.5	700.5/13.0	599.1/66.6	632.2/12.7
11	720.0/10.4	708.4/7.1	713.4/12.4	505.8/68.4	614.0/15.8
12	718.6/11.1	706.3/6.9	727.7/11.4	519.4/66.2	614.9/14.3
13	724.6/10.0	690.8/6.9	741.0/10.9	596.6/61.6	612.8/13.7
14	695.8/10.1	678.7/6.7	741.4/10.8	524.2/63.7	609.3/14.2
15	694.4/9.8	679.3/6.7	724.8/11.3	480.3/61.8	599.7/14.1
16	689.5/10.1	686.7/6.5	712.3/11.7	450.1/62.6	596.7/14.2
17	681.4/10.1	684.3/6.8	718.7/12.1	427.7/62.5	600.4/14.0
18	673.4/10.0	678.7/6.6	731.5/12.0	456.2/64.2	604.3/14.3
19	674.7/10.6	675.4/6.8	743.6/10.7	511.3/62.4	622.6/14.1
20	676.2/11.6	690.0/7.0	742.0/10.9	582.1/60.1	648.0/11.9
21	682.9/12.0	707.0/7.4	736.1/10.8	529.4/66.9	649.4/11.6
22	631.5/36.7	724.9/7.0	715.6/11.7	492.5/70.2	651.7/12.0
23	624.0/39.7	743.1/7.1	697.4/12.7	471.3/70.7	648.6/13.1
24	623.8/39.3	737.9/7.4	680.5/13.3	411.9/72.2	644.5/15.6

Appendix C

TABLE C.1 Emitting source selection hourly marginal emission rates/standard errors (kg CO_2eq/MWh).

Hour	AZPS	BPAT	CISO	DUK	ERCO	FPL
1	545.9/22.7	733.9/22.5	468.4/10.2	808.4/12.1	525.7/5.4	459.1/11.1
2	533.9/23.9	732.3/22.1	468.0/10.8	806.8/12.6	520.7/5.4	456.9/11.4
3	536.1/25.1	730.4/22.5	463.6/11.6	798.4/13.2	517.3/5.3	458.6/11.5
4	540.1/24.6	723.9/22.0	468.9/12.4	793.1/12.5	516.1/5.1	457.3/11.7
5	546.8/24.0	719.0/21.4	448.5/7.8	776.1/12.9	517.3/5.2	466.7/11.1
6	529.0/22.6	482.7/29.5	453.8/12.6	759.2/11.3	518.9/5.1	462.8/9.7
7	526.3/20.5	454.4/14.6	427.1/11.7	754.9/10.0	521.0/4.7	456.7/7.6
8	528.0/19.3	464.4/14.5	432.2/9.6	749.9/9.1	522.7/4.8	452.5/7.5
9	527.3/18.5	497.4/15.2	449.9/7.5	779.1/9.8	527.7/5.2	454.4/9.1
10	552.8/17.1	576.2/13.9	469.2/6.9	805.6/10.8	529.7/5.2	453.2/10.6
11	563.0/16.7	588.9/14.1	476.5/7.3	798.0/10.5	536.9/5.2	459.7/10.4
12	577.6/15.5	597.2/14.0	475.9/6.8	786.4/9.9	538.8/4.8	466.8/9.4
13	584.7/14.0	516.3/14.6	469.4/7.0	776.9/9.8	538.2/4.5	480.0/8.7
14	591.7/13.8	504.0/14.6	471.7/6.8	769.7/9.4	539.9/4.6	488.6/8.0
15	597.8/13.4	483.3/15.0	468.1/6.8	769.5/9.1	539.1/4.6	500.0/7.7
16	606.0/13.9	480.8/15.5	468.1/7.0	766.3/8.8	543.8/4.6	506.2/7.1
17	612.1/14.4	473.0/15.8	475.5/7.1	771.2/8.4	540.0/4.6	504.7/7.0
18	613.8/16.1	533.3/13.9	484.2/7.5	777.2/8.2	541.5/4.5	508.5/7.2
19	603.9/18.0	525.3/14.2	482.7/6.5	784.8/8.0	537.5/4.5	505.9/7.5
20	589.9/19.5	515.7/14.1	485.2/7.0	788.9/8.0	532.6/4.4	500.6/7.8
21	585.0/20.5	519.2/14.4	483.7/7.3	798.2/8.1	521.1/4.4	487.6/8.2
22	574.9/21.5	545.6/14.1	482.4/7.9	814.7/9.0	522.0/4.6	468.1/9.4
23	570.5/21.4	690.4/22.4	487.1/9.5	819.8/10.2	522.1/5.0	459.6/11.7
24	575.8/21.3	928.6/22.7	486.0/10.3	814.0/10.3	524.0/5.2	430.8/11.4

TABLE C.2 Emitting source selection hourly marginal emission rates/standard errors (kg CO_2eq/MWh).

Hour	IPCO	ISNE	MISO	NEVP	NWMT	NYIS
1	754.1/17.0	442.5/8.8	742.6/7.2	525.2/11.6	1010.3/5.5	487.3/11.3
2	749.1/16.8	433.9/8.6	727.9/7.3	540.9/11.7	1014.3/5.8	470.4/11.3
3	759.0/16.8	432.4/8.8	722.9/7.4	552.2/12.0	1010.2/6.0	466.2/11.6
4	760.8/16.5	434.9/8.9	727.7/7.7	563.6/12.4	1007.7/5.9	460.7/11.6
5	758.6/16.5	442.6/9.1	741.4/7.6	559.8/12.9	1013.8/6.1	458.6/12.0
6	749.7/17.4	418.6/7.2	759.1/6.8	552.9/13.5	1015.3/5.9	480.7/14.4
7	747.8/18.1	427.8/4.1	759.4/6.4	527.3/13.1	1005.2/8.9	486.4/13.0
8	753.7/18.0	420.1/3.8	769.3/6.6	518.6/11.4	1013.6/5.4	481.8/11.0
9	746.6/17.0	424.2/3.9	777.1/7.2	514.1/10.6	1024.3/5.3	519.7/11.5
10	754.3/16.0	424.5/3.8	777.3/7.3	518.7/10.2	1031.9/4.6	529.4/11.5
11	765.0/15.7	421.0/3.5	780.6/6.9	518.1/10.0	1030.8/4.6	525.1/11.1
12	757.1/15.1	428.1/5.7	773.7/6.5	509.5/10.2	1025.4/4.7	529.4/11.1
13	757.4/14.8	428.7/5.7	778.3/6.5	514.5/9.6	1031.4/4.6	529.4/11.2
14	745.0/14.8	429.0/5.7	778.9/6.6	520.2/9.2	1033.2/4.6	522.1/11.0
15	745.0/15.4	429.5/5.8	778.5/6.7	524.4/9.7	1025.8/4.3	524.0/10.7
16	738.3/15.5	429.1/3.6	783.1/9.2	524.9/10.7	1022.7/4.6	534.8/10.7
17	728.4/15.3	432.7/3.8	781.8/9.4	538.0/14.6	1025.2/4.4	563.6/9.9
18	730.7/15.1	437.2/3.8	773.4/9.3	555.9/15.3	1027.6/4.5	569.2/9.7
19	748.5/15.5	440.9/3.9	774.1/8.9	577.7/17.6	1024.6/4.4	574.5/10.2
20	756.7/16.8	437.6/3.8	778.9/9.0	576.0/18.9	1013.0/5.9	571.7/10.4
21	757.9/17.3	436.1/3.7	780.2/9.2	560.5/19.9	1011.9/6.2	563.3/10.5
22	752.8/17.6	447.7/7.3	784.6/7.0	510.9/14.2	1025.0/4.3	568.0/10.3
23	755.7/18.9	435.7/4.2	777.6/7.0	515.1/12.9	1020.1/4.3	536.0/11.7
24	751.5/18.0	448.5/8.6	766.6/7.3	520.0/11.9	986.2/10.0	517.5/11.8

TABLE C.3 Emitting source selection hourly marginal emission rates and standard errors (kg CO_2eq/MWh).

Hour	PACE	PJM	SOCO	SWPP	TVA
1	771.4/13.4	723.6/7.9	664.8/13.3	769.8/7.7	645.3/17.6
2	765.5/14.2	712.8/8.4	652.8/13.3	766.7/7.7	637.1/17.5
3	781.0/14.6	702.7/9.1	638.4/13.1	764.8/7.8	620.2/16.8
4	785.0/13.6	694.6/9.5	637.1/13.2	762.9/7.5	617.3/15.9
5	780.4/13.2	686.3/9.5	643.0/12.9	750.8/7.7	617.7/15.3
6	765.5/13.1	680.3/8.7	645.9/11.6	743.0/7.8	614.6/14.5
7	729.8/12.7	673.4/8.2	649.0/11.4	739.5/7.8	611.4/15.2
8	733.2/11.9	683.3/7.2	656.1/12.3	742.1/7.7	610.6/13.2
9	737.4/13.1	711.6/6.9	695.4/13.4	754.3/8.1	615.5/13.4
10	764.0/11.2	735.3/7.1	718.9/12.7	754.5/8.2	634.1/12.7
11	779.6/10.0	737.1/6.6	728.3/12.2	761.1/7.3	646.7/12.5
12	774.3/10.9	740.7/6.5	739.0/11.3	763.9/7.3	658.2/11.9
13	784.9/9.6	737.4/6.6	745.3/10.9	765.2/7.7	663.1/11.7
14	758.2/9.9	733.6/6.4	746.6/10.8	769.7/7.7	659.3/12.1
15	753.7/9.4	738.1/6.5	746.8/11.0	770.0/7.7	656.1/12.1
16	753.7/9.9	741.3/6.0	748.4/11.2	774.9/7.8	659.6/11.9
17	743.8/9.8	733.8/6.2	755.5/11.2	766.3/8.2	655.4/11.7
18	736.6/9.8	730.6/6.2	754.2/11.0	765.4/8.0	651.1/12.4
19	734.9/10.3	732.6/6.2	746.9/10.7	764.0/7.7	655.5/11.9
20	728.8/11.1	741.0/6.4	743.2/10.9	764.7/8.5	651.1/11.9
21	727.1/11.6	748.5/6.7	736.2/10.8	769.0/8.6	652.3/11.6
22	727.8/12.2	755.4/6.8	715.6/11.7	766.0/8.5	652.6/12.0
23	741.2/12.7	761.2/7.3	697.6/12.7	772.9/8.1	649.4/13.1
24	762.2/13.7	750.7/7.5	680.8/13.3	772.5/7.8	645.1/15.6